

Modelling and experimental study of low temperature energy storage reactor using cementitious material

Khadim Ndiaye, Stéphane Ginestet, Martin Cyr

▶ **To cite this version:**

Khadim Ndiaye, Stéphane Ginestet, Martin Cyr. Modelling and experimental study of low temperature energy storage reactor using cementitious material. Applied Thermal Engineering, 2017, 110, pp.601–615. 10.1016/j.applthermaleng.2016.08.157 . hal-01847545

HAL Id: hal-01847545

https://hal.insa-toulouse.fr/hal-01847545

Submitted on 6 Mar 2020

HAL is a multi-disciplinary open access archive for the deposit and dissemination of scientific research documents, whether they are published or not. The documents may come from teaching and research institutions in France or abroad, or from public or private research centers.

L'archive ouverte pluridisciplinaire **HAL**, est destinée au dépôt et à la diffusion de documents scientifiques de niveau recherche, publiés ou non, émanant des établissements d'enseignement et de recherche français ou étrangers, des laboratoires publics ou privés.

Modelling and experimental study of low temperature energy storage reactor using cementitious material

Khadim Ndiaye, Stéphane Ginestet*, Martin Cyr

Université de Toulouse-INSA-UPS; Laboratoire Matériaux et Durabilité des Constructions de Toulouse, (* sgineste@insa-toulouse.fr)

Abstract

Renewable energy storage is now essential to enhance the energy performance of buildings and to reduce their environmental impact. Most adsorbent materials are capable of storing heat, in a large range of temperature. Ettringite, the main product of the hydration of sulfoaluminate binders, has the advantage of high energy storage density at low temperature, around 60°C. The objective of this study is, first, to predict the behaviour of the ettringite based material in a thermochemical reactor during the heat storage process, by heat storage modelling, and then to perform experimental validation by tests on a prototype. A model based on the energy and mass balance in the cementitious material was developed and simulated in MatLab software, and was able to predict the spatiotemporal behaviour of the storage system. This helped to build a thermochemical reactor prototype for heat storage tests in both the charging and discharging phases. Thus experimental tests validated the numerical model and served as proof of concept.

Keywords: thermochemical storage, ettringite, hydration-dehydration, modelling, reactor prototype

Nomenclature

a_g thermal diffusivity of steam (m^2/s)
a_f thermal diffusivity of fluid (m^2/s)
c_w specific heat of liquid water (J/(kg.K))
c_g specific heat of water vapour (J/(kg.K))
c_s specific heat of material (J/(kg.K))
c_h volumetric heat of three phases (J/(kg.K))
d diameter (m)
dz length of longitudinal mesh (m)
dr_f length of radial mesh in the tube (m)
dr_s length of radial mesh in material (m)
D_v diffusion coefficient of stream (m^2/s)
RH relative humidity (%)
K gas permeability of material (m^2)
K_{LDF} mass transfer coefficient (1/s)
L length of the reactor (m)
M molar mass of adsorbed phase (kg/mol)
n_f number of radial meshes in material
n_s number of radial meshes in material
n_z number of longitudinal meshes
NUT number of transfer units
p water vapour pressure (Pa)
p_{vs} saturation vapour pressure (Pa)
q water uptake (kg/m^3)
q_{equ} water uptake at equilibrium (kg/m^3)
r radial coordinate (m)
R gas constant (J/(mol.K))
R_1 inner radius of the metal tube (m)
R_2 outer radius of the metal tube (m)
R_3 outer radius of the material (m)
t time (s)
T temperature (K)
u gas phase velocity in the material (m/s)
v fluid velocity in the metal tube (m/s)
z axial coordinate (m)

Greek letters

ε porosity
ρ density (kg/m^3)
λ thermal conductivity (W/(m.K))
ΔH heat of sorption (J/kg)
μ dynamic viscosity (Pa.s)

Subscripts

equ equilibrium
f heat transfer fluid
g gaseous phase (water vapour)
h three phases homogenized
in inlet
LDF linear driving force
m maximum
s solid material
w liquid phase (water)
0 initial

1. Introduction

The use of renewable energy in the building sector can considerably reduce its environmental and socio-economic impacts. The excess solar energy in summer could be stored and then released later in autumn or winter, in order to decrease the phase shift between solar radiation and thermal energy needs. Many heat storage materials can be used in the building sector in order to avoid the phase shift between solar radiation and thermal energy demand. Thermal energy storage in general, and phase change materials (PCMs) in particular, have been a main topic in research for the last 20 years [1], but they usually allow to reduce short phase shifts. Another way of reaching this goal of seasonal thermal heat storage could be to explore thermochemical storage, and to use a particular shape of cementitious materials. Indeed, ettringite, a common hydrated phase found in cement-based materials, has the advantage of high energy storage density at low temperature (60°C) compared to existing adsorbent materials such as zeolites [2,3]. This component is found in small quantities in Portland cement paste (around 10 %), while high ettringite content (40-80%) can be reached by calcium sulfoaluminate cement hydration [4].

Concrete solutions for thermal energy storage are usually based on sensible heat transfer and thermal inertia [5,6], and sometimes they are enhanced with PCMs solutions [7,8]. An ettringite based material, capable of storing thermal energy by a reversible dehydration/hydration cycle, was produced by hydration of a mixture of sulfoaluminate clinker, anhydrite and aluminium powder [9]. Thermal energy storage by ettringite material is a physicochemical process usable in both the short (daily, weekly) and long (seasonal) term. In the charge phase, heat is stored by endothermic processes (desorption and dehydration) and is not restored as long as the material remains dry. In the discharge phase, the heat stored in the material is released by exothermic adsorption (adsorption and hydration). The chemical part of the energy storage process is related to the reversible conversion of ettringite ($3CaO.Al_2O_3.3CaSO_4.30H_2O$) to metaettringite ($3CaO.Al_2O_3.3CaSO_4.12H_2O$).

The first objective of this study is to predict the behaviour of the ettringite-based material in a thermochemical reactor (cylindrical adsorber) during the heat storage process, by simulating the spatiotemporal variation of the temperature and the water vapour pressure inside the storage material. Then the second aim is to carry out an experimental validation by testing a prototype. To reach this goal, the physical, thermal and hygrometric properties of the material were measured, using standardized tests, and used in an energy storage model [10,11].

Several 1D or 2D energy storage models based on adsorbent materials such as zeolites can be found in the literature [12,13,14,15,16]. To predict the spatiotemporal behaviour of the storage system during heat charging and discharging, a two-dimensional model taking the specificities of

cementitious material into account was developed. The heat and mass balance in the thermochemical reactor (cylindrical adsorber) generated a system of non-linear and strongly coupled differential equations. They were solved numerically, first by spatial discretization using the finite difference method [17], and then by temporal integration of state variables (temperature and water vapour pressure) using the Gear method [18,19,20] in MatLab.

The simulation of this model using measured properties of the ettringite material (physical, thermal and hygrometric properties) provided the evolution of temperature and water vapour partial pressure in the thermochemical reactor during charge and discharge of heat. The evolution of the variables observed during charge and discharge of heat corresponded to the desorption and adsorption phases, respectively. This numerical study gave a complete prediction that allowed us not only to understand the material behaviour better, but also to determine the optimal operating conditions of heat storage. This helped to build the thermochemical reaction prototype for heat storage tests in both the charging and discharging phases.

To store solar heat (daily or seasonal storage), for example, it was necessary to connect the thermochemical reactor with a heat source (e.g. solar collector) to charge it in the storage phase. During the discharging phase, a humidification source was required to release the heat. To perform the storage tests in the laboratory, the reactor was connected to an electric water heater and a humidifier (bubbler) simulating the charge and discharge of heat, respectively. The test bed installed in the laboratory reproduced the storage system functioning during both phases. The comparison between numerical and experimental results validated the numerical model and served as proof of concept.

2. Thermochemical reactor description and principle

The two-dimensional modelling of heat storage was based exclusively on the thermochemical reactor, which was the key element of the heat storage system. The thermochemical reactor (Figure 1) consisted of a thin metal tube (R_2 - R_1) where the heat transfer fluid (hot water) heated the ettringite-based material placed around the tube (ettringite material between R_2 and R_3) during the charging period. The ettringite material was then insulated from the surrounding environment to avoid heat loss.

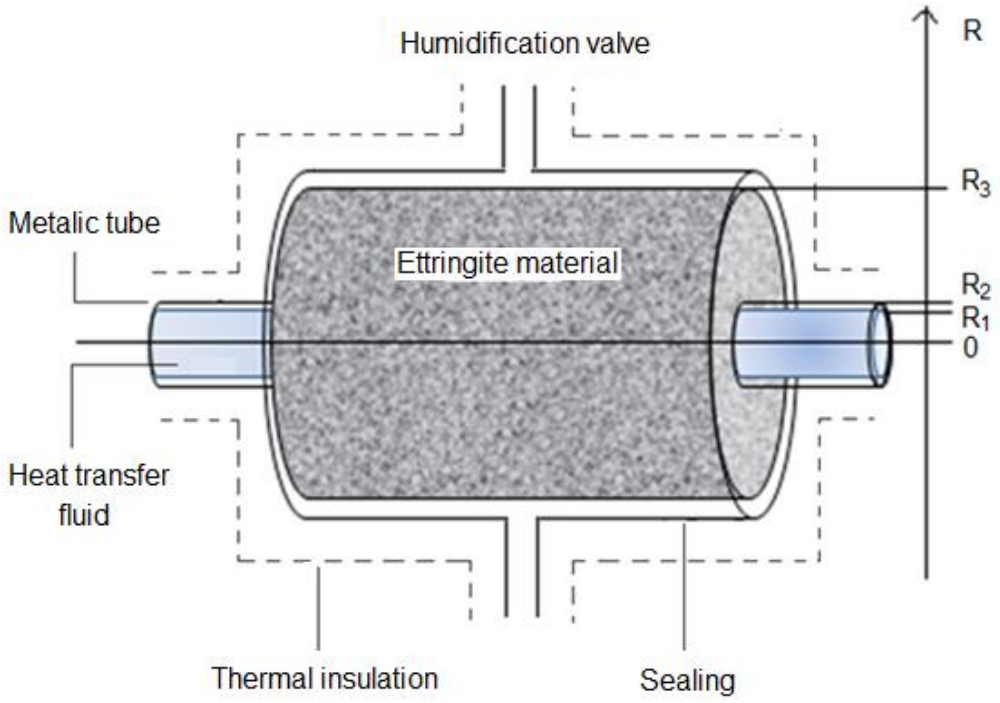


Figure 1: Thermochemical reactor with ettringite based material

A cylindrical adsorber, filled with zeolite, is often used to store heat using a longitudinal humidification system [12,16]. Longitudinal humidification means that the water vapour is introduced at both ends of the storage material. That is to say, the humidified gas (water in vapour phase) circulates through the material porosity in the longitudinal direction (z). The moist input gas (z = 0) dries progressively as a result of the adsorption of water vapour by the material and the outlet gas (z = L) is thus dry. Furthermore, a radial humidification system, i.e. around the storage material, has the advantage of quickly creating a uniform water vapour pressure in the adsorber [13,21]. Therefore, a thermochemical reactor filled with ettringite-based material with a radial humidification system was selected (Figure 1). The simulation of this thermochemical reactor during the heat storage process required the prior description of its functioning and the phenomena taking place within it.

In the charging phase, the heat (from water at 60° C, supplied by a boiler or a solar thermal collector, for example) is transferred to the reactor via the heat transfer fluid (hot water in the central metal tube, Figure 2). Heating the ettringite-based material causes its endothermal desorption and ettringite ($3CaO.Al_2O_3.3CaSO_4.30H_2O$) is converted to metaettringite ($3CaO.Al_2O_3.3CaSO_4.12H_2O$) by endothermal dehydration. Thus the heat is stored (Figure 2). The resulting cooled heat-transfer fluid continues to circulate and the desorbed water vapour is moved out of the adsorber. The stored heat is saved as long as the thermochemical reactor is isolated from water vapour flux.

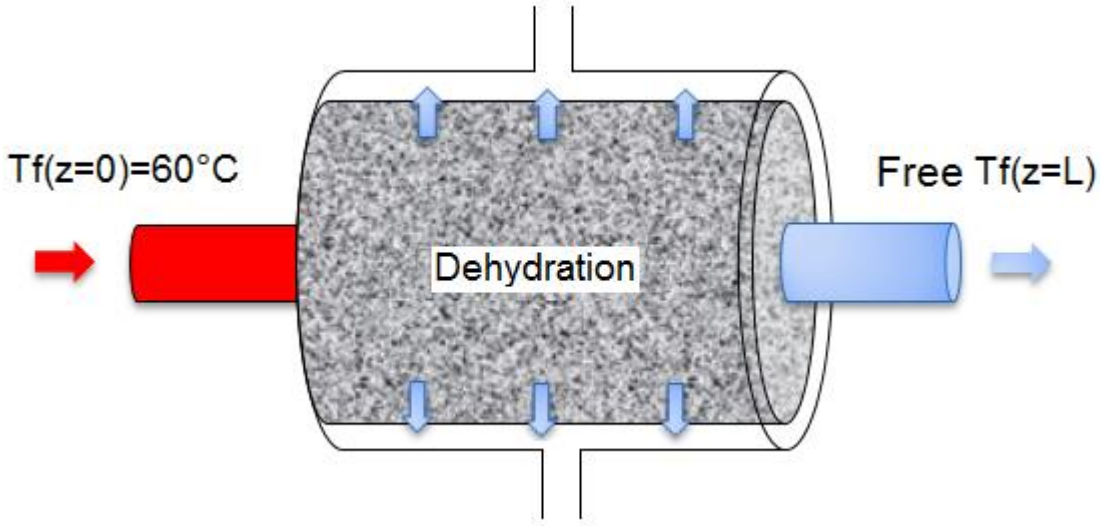


Figure 2: Thermochemical reactor during charging phase

During the discharging phase, the stored heat is recovered by a radial humidification circuit, which causes the exothermal adsorption of water molecules on ettringite crystals (and thus hydration) (Figure 3).

However, the main problem of using this material is that ettringite decomposes over time in the presence of carbon dioxide (CO_2), by carbonation [22]. It is necessary to avoid the presence of CO_2 to ensure the stability of the ettringite. Therefore, in our model, moist nitrogen was used instead of moist air to humidify the material, avoiding carbonation, in the heat restitution phase.

Nitrogen is used here only to be a neutral medium to carry the water vapor. If air is used as a medium, it is possible to avoid the presence of CO_2 by using a filtration membrane blocking the CO2 at the prototype inlet, by enhancing the material's behaviour to carbonation (development underway in the laboratory), or by using a sealed prototype (sealed flow with air).

In the prototype, the humidified nitrogen passed through the material radially, allowing the sorption equilibrium to be reached quickly on the outer face of the material (side face R_3 in Figure 1). The initially dry material adsorbed water vapour and the metaettringite ($3CaO.Al_2O_3.3CaSO_4.12H_2O$) was converted to ettringite ($3CaO.Al_2O_3.3CaSO_4.30H_2O$) by endothermal dehydration.

The physical adsorption and chemical rehydration (exothermic) released the stored heat **(**Figure 3**)**. The metaettringite was converted to ettringite by exothermal rehydration. The heat generated was moved outside the reactor by the cold fluid (water at 20°C) which continued to circulate in the metal tube, and could be used via a heat exchanger in a secondary heating system or a mechanical ventilation system for building applications.

The phenomena occurring in the material during the heat storage cycle were modelled by a system of differential equations that correctly described the spatiotemporal behaviour of the thermochemical reactor.

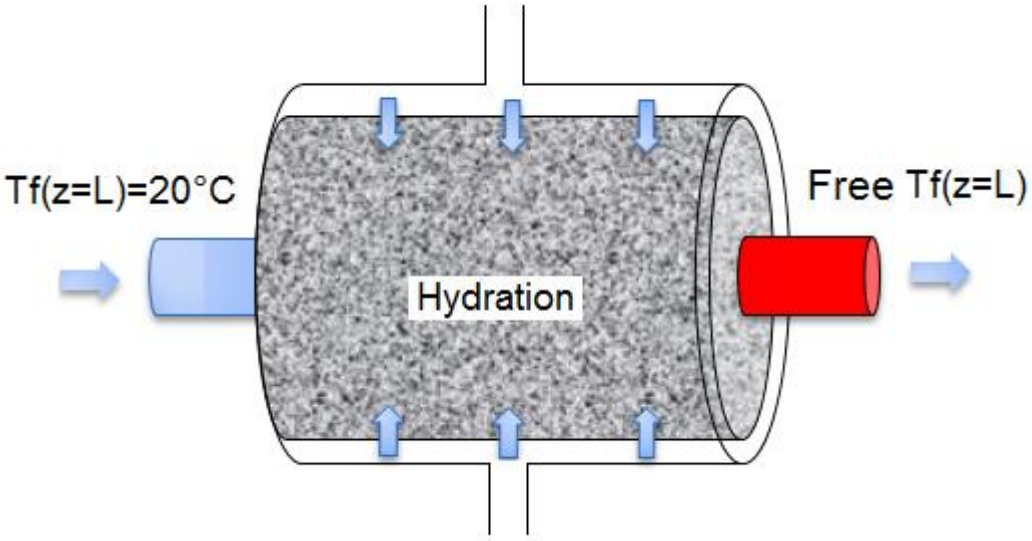


Figure 3: Thermochemical reactor during discharging phase

3. Mathematical model of the transfer phenomenon in the cementitious material

3.1. Modelling assumption

To write the mathematical formulation, some assumptions had to be made. The literature commonly considers adsorbent materials in powder form so, to account for the specificities of the monolithic cementitious material, some complementary assumptions were necessary.

First, the thermal effect of impurities present in the cementitious material was neglected: the potential contribution of secondary hydrates such as $Al(OH)_3$ was not taken into account. Secondly, the ettringite was considered not to be carbonated as nitrogen gas was used in the closed storage system (no air with carbon dioxide). Then, the sorption isothermal model described water adsorption by ettringite at equilibrium conditions: the transverse walls of the absorber ($z = 0$ and $z = L$) were assumed adiabatic, unlike the metal tube, and it was assumed that there was no accumulation of energy in the thin metal tube.

Finally, the assumption of instantaneous sorption equilibrium usually accepted for the adsorbent materials [12,16] was not appropriate for this cementitious material with slower kinetics. In fact, these previous authors considered that the sorption equilibrium was reached at any time, that is to say, the amount of adsorbed water was independent of time and was equal to the amount of adsorbed water at equilibrium. This was suitable for storage materials such as zeolites with fast

sorption kinetics (of the order of a microsecond). However, an experimental test showed very slow sorption kinetics for the material used here [10] and hence it was necessary to establish a relationship (sorption kinetics) to calculate the amount of water adsorbed over time (q (t)) from the amount of water reached at sorption equilibrium (q_{equ} provided by sorption isotherms).

The simplified Linear Driving Force (LDF) diffusion model [23,24,25,26] was used to model the sorption kinetics here:

$$\frac{\partial q(t)}{\partial t} = K_{LDF}\left(q_{equ} - q(t)\right) \quad (1)$$

with $K_{LDF} = 8\frac{D_V}{R^2}$

with $q(t)$ the water uptake at time t from the Linear Driving Force LDF model (kg/m^3); D_v the diffusion coefficient of stream measured in the laboratory, $D_v = 7.14 \times 10^{-9}$ m^2/; R the radius of the material in the prototype; q_{equ} the equilibrium water uptake from sorption isotherms (kg/m^3).

The analytical solution of the LDF method is given by Equation 2 (Figure 4).

$$q_{LDF}(t) = q_{equ}\left(1 - \exp\left(-8\frac{D_V}{R^2}.t\right)\right) \quad (2)$$

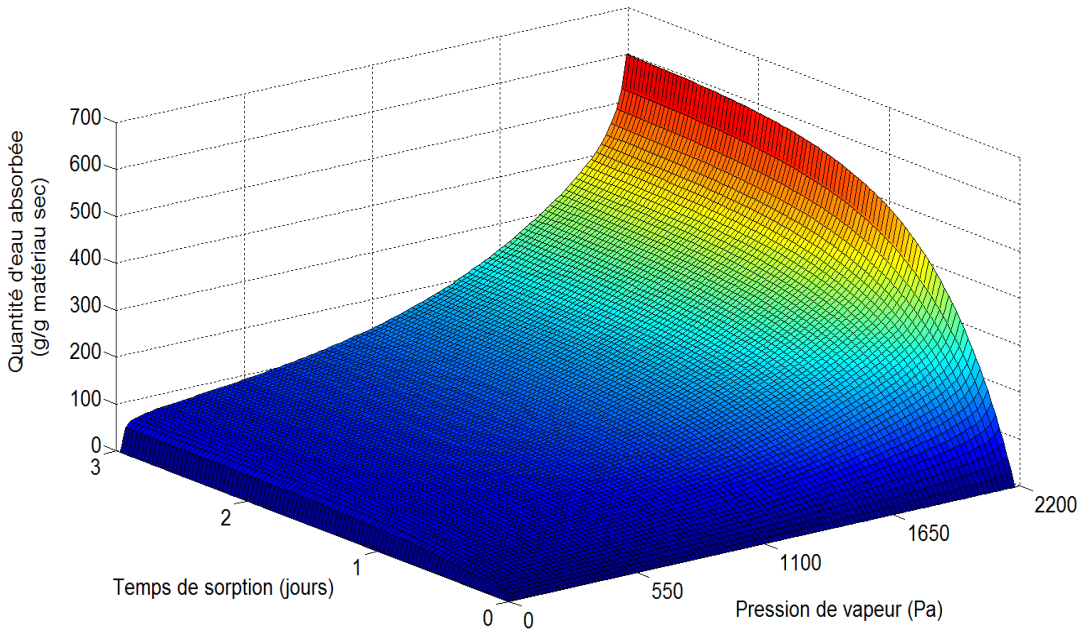


Figure 4 : Sorption kinetic of the material at T= 20°C (LDF model fitted with experimental parameters)

It was assumed that Darcy's law applied in porous media such as these cementitious materials. This law allowed the velocity of the gas (water vapour) to be determined in the material porous network:

$$u = -\frac{K}{\mu}\nabla \mathrm{p} \tag{3}$$

The gaseous phase (water vapour) was taken to be ideal gas:

$$\rho_g = \frac{M.p}{R.T} \tag{4}$$

The liquid flow profile followed Poiseuille's Law:

$$v(r) = v_{max}\left(1 - \left(\frac{r}{R_1}\right)^2\right) \tag{5}$$

3.2. Energy and mass balance in the reactor

The state variables were the temperature of the heat transfer fluid in the metal tube, T_f (r,z,t), and the temperature, T(r,z,t), and water vapour pressure, p(r,z,t), in the ettringite material. Their evolution described the dynamic behaviour of the thermochemical reactor. The spatiotemporal evolution of these variables was obtained by solving the heat storage model based on the energy and mass balance in the ettringite material.

Several energy storage models (1D or 2D) using zeolites have already been presented in the literature [12,13,14,15,16]. In this study, the aim of the model was to describe the dynamic behaviour of ettringite-based material during the heat storage process by using the spatiotemporal

evolution of the temperature, T(r, z, t), and the water vapour pressure, p(r, z, t), in the cementitious material. The two-dimensional model was built in cylindrical coordinates (Figure 5). The differential equations based on energy and mass balance in the thermochemical reactor were:

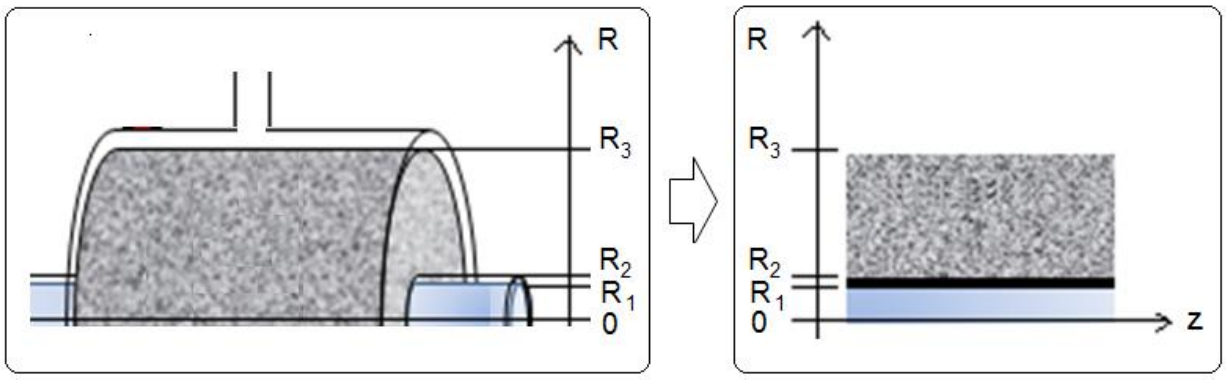


Figure 5: Two-dimensional model of thermochemical reactor

- Energy balance in the heat transfer fluid

$$\frac{\partial T_f}{\partial \mathrm{t}} + v(r).\nabla T_f - a_f\,\nabla^2 T_f = 0 \qquad (6)$$

$$\text{with } v(r) = 2v_{mean}\left(1 - \left(\frac{r}{R1}\right)^2\right);\ a_f = \frac{\lambda_f}{\rho_f.c_f}$$

- Energy balance in the cementitious material

$$\frac{\partial (c_h\,T)}{\partial t} + \nabla\left(\rho\,u\,c_g T\right) - \nabla(\lambda\,\nabla T) = (1-\varepsilon)\Delta H\frac{\partial \mathrm{q}}{\partial \mathrm{t}} \qquad (7)$$

$$\text{with } c_h = \varepsilon\,\rho_g\,u\,c_g + (1-\varepsilon)(\rho_s c_s + q.c_w);\ u = -\frac{K}{\mu}\nabla \mathrm{p}$$

- Mass balance in the cementitious material

$$\varepsilon\,\frac{\partial \rho}{\partial t} + \nabla\,(\rho\,u) = -(1-\varepsilon)\frac{\partial q}{\partial t} \qquad (8)$$

- Sorption kinetics in the cementitious material

$$\frac{\partial q}{\partial t} = K_{LDF}(q_{equ} - q) \qquad (9)$$

- The connecting condition at the interface between the heat transfer fluid and the metal tube

$$\frac{\partial T_f}{\partial r}(R_1, z, t) = \frac{\lambda_m}{\lambda_f}\frac{1}{R_1}\frac{T_f(R_1, z, t) - T(R_2, z, t)}{ln(\frac{R_1}{R_2})} \qquad (10)$$

- The connecting condition at the interface between the metal tube and the cementitious material

$$\frac{\partial T}{\partial r}(R_2, z, t) = \frac{\lambda}{\lambda_m}\frac{1}{R_2}\frac{T_f(R_1, z, t) - T(R_2, z, t)}{ln(\frac{R_1}{R_2})} \quad (11)$$

3.3. Boundary conditions and initial conditions

The boundary and initial conditions allowed the operating conditions of the reactor to be reproduced during the charging phase and the discharging phase. These conditions were different in the two phases. At the initial state ($t = 0\ s$) of each phase (charging or discharging), the system was in thermal equilibrium:

$$T_f(r, z, 0) = T(r, z, 0) = T_{room} \quad (12)$$

In the charging phase, the ettringite material was initially saturated, the relative humidity was maximal within the material porosity, and the water vapour pressure was taken as the saturation vapour pressure at room temperature:

$$\begin{cases} p(r, z, 0) = p_{vs}\ (T_{room}) \\ q(r, z, 0) = q_{equ}\ \left(T_{room},\ p_{vs}(T_{room})\right) \end{cases} \quad (13)$$

The advantage of this type of storage is that the intermediate stage (cooling phase), between charging and discharging, can last several months without loss of sorption heat (seasonal storage). The stored heat was saved as long as the thermochemical reactor was isolated from water vapour flux. The material should be kept dry in intermediate stage, so the initial condition for the discharging phase was:

$$\begin{cases} q(r, z, 0) = q_0 = 0\ kg/m^3 \\ p(r, z, 0) = p_0 = 0\ Pa \end{cases} \quad (14)$$

The symmetry condition with the heat transfer fluid was:

$$\frac{\partial T_f(r, \mathrm{z}, 0)}{\partial z} = 0 \quad (15)$$

During both phases (charging and discharging), the side walls at the material level (z = 0 and z = L) were considered adiabatic and impermeable:

$$\begin{cases} \dfrac{\partial T(r,0,t)}{\partial z} = \dfrac{\partial T(r,\mathrm{L},t)}{\partial z} = 0 \\ \dfrac{\partial p(r,0,t)}{\partial z} = \dfrac{\partial p(r,\mathrm{L},t)}{\partial z} = 0 \end{cases} \quad (16)$$

The boundary conditions during both phases are given in Table 1.

Table 1: Boundary conditions during charging phase and discharging phase

	Charging phase (desorption)	Discharging phase (adsorption)
z = 0	$\boldsymbol{T_f(r,0,t) = T_{heat} = 60\,℃}$ $\dfrac{\partial T(r,0,t)}{\partial z} = 0$ $\dfrac{\partial p(r,0,t)}{\partial z} = 0$	$T_f(r,0,t) = T_{room} = 20\,℃$ $\dfrac{\partial T(r,0,t)}{\partial z} = 0$ $\dfrac{\partial p(r,0,t)}{\partial z} = 0$
z = L	$Free\ T_f(r,L,t)$ $\dfrac{\partial T(r,L,t)}{\partial z} = 0$ $\dfrac{\partial p(r,L,t)}{\partial z} = 0$	$Free\ T_f(r,L,t)$ $\dfrac{\partial T(r,L,t)}{\partial z} = 0$ $\dfrac{\partial p(r,L,t)}{\partial z} = 0$
r = R_3	$p(r_3,z,t) = p_0 = 0\ Pa$ $\dfrac{\partial T(r_3,z,t)}{\partial z} = 0$	$\boldsymbol{p(r_3,L,t) = p_{vs}(T_{room})}$ $\dfrac{\partial T(r_3,z,t)}{\partial z} = 0$

After this detailed description of coupled nonlinear differential equations based on heat and mass balance in the storage materials, the resolution method is explained in Section 4.

4. Numerical method

Various numerical methods were used in solving this mathematical model. Instead of multiphysics commercial software, a classic method was used with an implementation in MatLab®. The numerical resolution was based on a spatial discretization by finite difference method [17] and time integration of the derivatives of state variables. Temporal integration was performed using the Gear method [18,19,20].

4.1. Spatial discretization and time integration

It was necessary to first solve the system of coupled nonlinear differential equations in order to predict the thermochemical reactor behaviour. The implicit second-order finite difference scheme was used to discretize the two-dimensional space [17]. The spatial derivatives of nonlinear equations were approximated by their limited development functions of second order (Taylor series). The space in the reactor was discretized by longitudinal meshes (z axis), radial meshes were used in the heat transfer fluid and in the cementitious material. So the space was divided by:

- n_z number of longitudinal intervals, with length $dz = \frac{L}{n_z}$,
- n_f number of radial intervals in the heat transfer fluid, with length $dr_f = \frac{R_1}{n_z}$,
- n_s number of radial intervals in the cementitious material, with length $dr_s = \frac{R_3 - R_2}{n_s}$

The problem of the temporal integration was the stiffness of the system, that is to say, the fact that it comprised different dynamics. System stiffness can cause severe loss of numerical solution accuracy [17]. This type of system requires a robust integration method able to take all the dynamics of the system into account.

The Gear method is a time integration algorithm with time steps that adapt according to each dynamics of stiff differential equations [18,19,20,27]. This auto-adaptive implicit algorithm allows the time step to be selected and the order to be changed automatically. The solver ODE15s in MatLab®, based on the Gear method, was used here to perform the temporal integration of the stiff equation system with an absolute error tolerance of 10^{-6}.

In fact, the time step was adapted to the fastest dynamics at a given time. So, even ephemeral variations of state variables (temperature and water vapour pressure) would not be neglected in the simulation. Before the temporal integration, all spatial derivatives of the system were first discretized, and then the system was written in standard form (equation 17).

$$\frac{dX}{dt} = f(X) \tag{17}$$

with X a column matrix containing all the state variables: the fluid temperature (T_f), and the temperature (T) and water vapour pressure (p) within the cementitious material.

The resolution procedure [17] was based on a first iteration using the initial conditions. Then the equations system was solved to find variables at the second iteration and updated nonlinearity terms. This procedure was repeated until the convergence criterion was reached.

4.2. Numerical scheme verification

Sun et al. [12] modelled a cylindrical adsorber with a central metal tube inside a bed of zeolite 13X. They assumed that the heat and mass transfer occurred exclusively in the longitudinal direction of the cylindrical reactor (one-directional exchanges along the z axis). To solve the differential equations, they used the finite method of order 3 based on a Crank-Nicolson scheme to discretize the time and space of their one-dimensional model (50 discrete grids and time step of 1 s). They also resolved their simplified model analytically (Laplace transform). Their discretization scheme was verified by comparison between the analytical and numerical solutions (Figure 6).

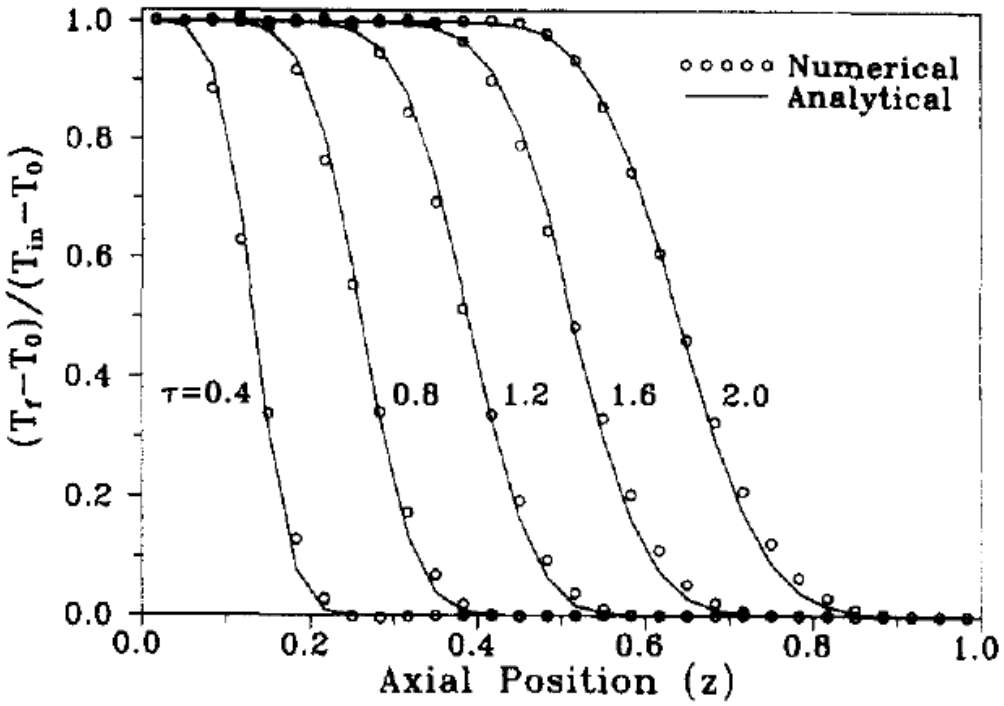


Figure 6: Analytical and numerical solution for the method of Sun et al. [12]

To verify our numerical scheme following the same approach, this one-dimensional model was solved with our numerical method described in section 4.1, i.e., spatial discretization using a 2nd order finite difference method and time integration using the Gear method. Then the numerical simulation was performed using the parameters of zeolite 13X [12]. The analytical model was also solved. The numerical and analytical results are compared in Figure 7. The temperature evolution over time from our numerical scheme was in accordance with that obtained with the analytical equation (Figure 7).

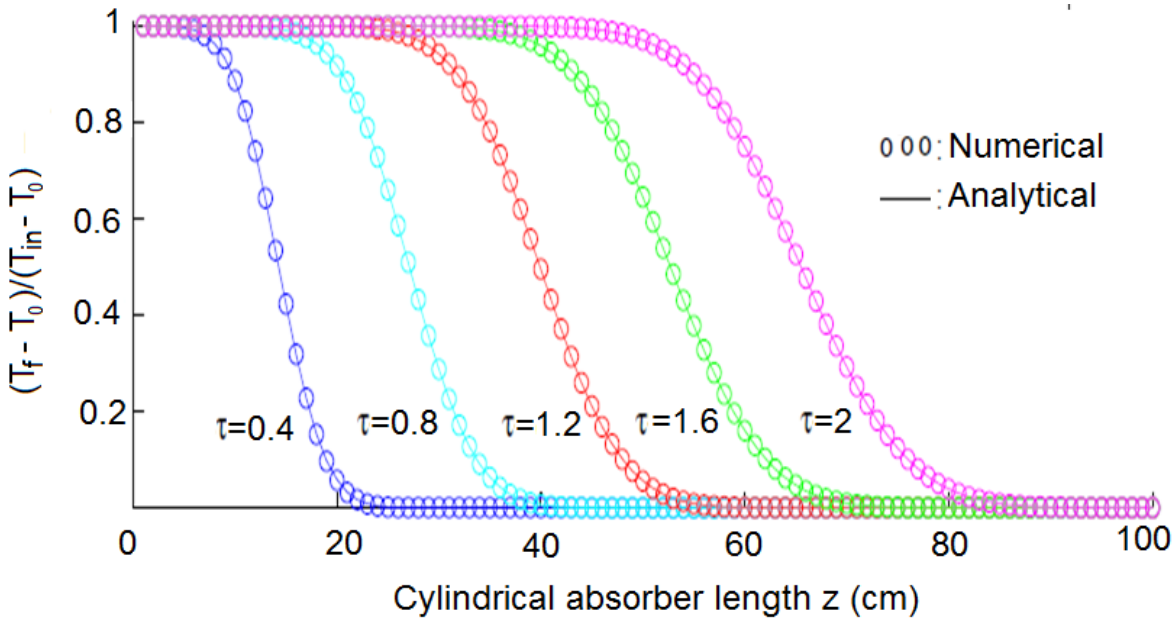


Figure 7: Analytical and numerical solution from our method

This proved that the numerical scheme allowed us to sufficiently describe the phenomena taking place in the thermochemical reactor during the heat storage process. The discretization error was the difference between the exact solution of the mathematical model and that of the discretized system [17]. Analytical and numerical solutions were assumed to be the exact solution of the mathematical model and that of the discrete system, respectively. The absolute error curve between analytical and numerical solutions confirmed the stability of the numerical scheme with a maximum error of about 2.10^{-3} (Figure 8). Figure 8 shows a decrease of absolute error over time and bed length of the cylindrical absorber.

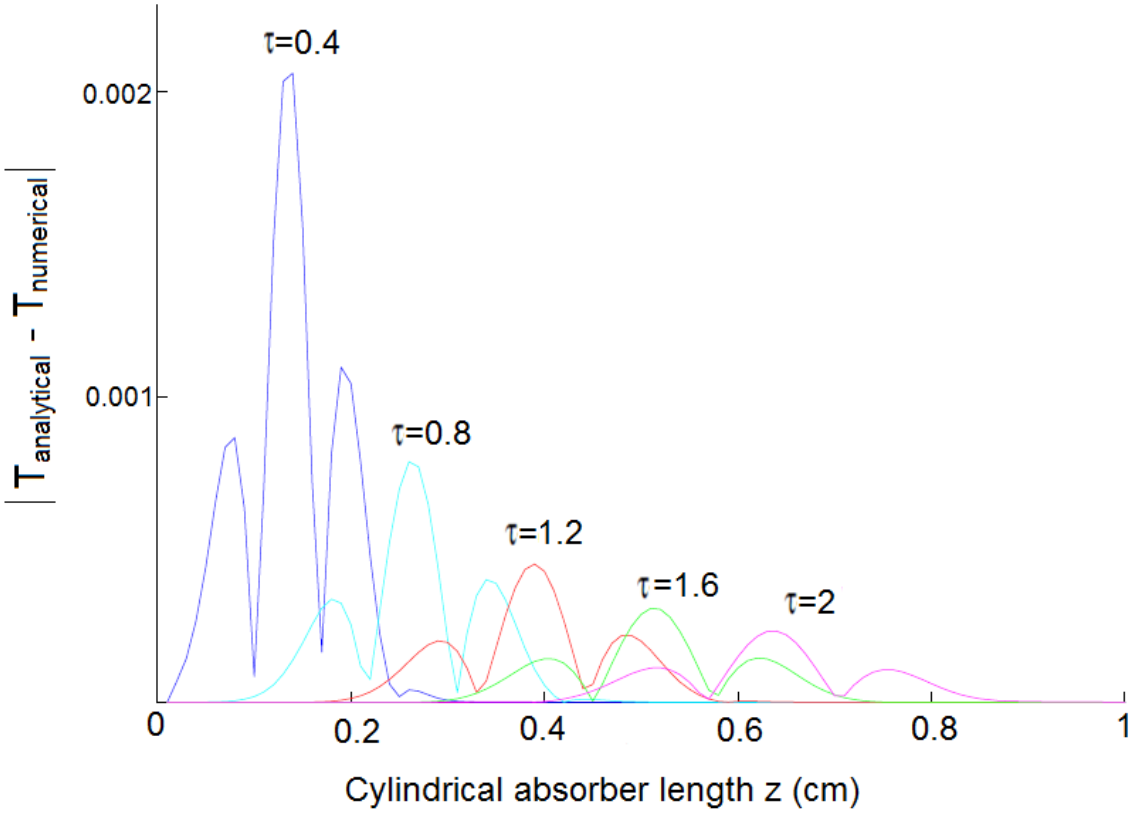


Figure 8: Absolute error between numerical and analytical solutions

These results show that our numerical scheme correctly describes the evolution of the phenomena that take place in a thermochemical reactor having the form of a cylindrical absorber.

5. Simulation results

The model simulation required input parameters that were intrinsic properties of the cementitious material (physical, thermal and hygrometric properties). These parameters were measured in the laboratory using laboratory devices, following standardized tests [10].

5.1. Model parameters

To perform the heat storage simulation in the thermochemical reactor (cylindrical adsorber) filled with the cementitious material, it was necessary to first measure its properties, which were the input parameters of the model.

5.1.1. Sorption isotherm

One of the most important phenomena of the storage process is water vapour sorption in the material. This phenomenon is characterized by the sorption isotherm, that is to say, the evolution of water sorption at equilibrium (q_{equ}) with steam pressure in the material. It also depends on the temperature (q_{equ} (p, T)). Water uptake at equilibrium in the material decreases with the sorption

temperature so considering only a single sorption isotherm (20°C) would neglect the thermal effect on the sorption of water, hence the accuracy of the numerical model would decrease.

To take the effect of temperature into consideration, the vapour sorption isotherm of water was measured at three different temperatures (20, 33 and 50°C) [10]. The resulting sorption isotherms showed three successive phases: a phase of low relative humidity corresponding to a monolayer sorption phase, then a multilayer sorption phase, followed by a capillary condensation sorption phase (up to saturation) with high relative humidity.

The sorption model of Pickett [28] is an improved BET model taking these three sorption phases into account. Thus, in our study, the Pickett model was used to model the experimental sorption isotherms.

$$q_{equ}(HR,T) = \frac{q_m\, c}{(1-HR)} \frac{HR(1-HR^n) + b\, n\, HR^n(1-HR)}{(1-HR) + c(HR + b\, HR^n)} \qquad (18)$$

q_m, c, b and n were parameters depending on the material temperature. These parameters were obtained by minimizing the difference between model and experiment by the least squares method.

$q_m(T) = a_1.T^2 + a_2.T + a_3$;
$c(T) = a_4.T^2 + a_5.T + a_6$;
$b(T) = a_7.T^2 + a_8.T + a_9$;
$n(T) = a_{10}.T^2 + a_{11}.T + a_{12}$;

The resulting parameters were:
$a_1 = 7.35962.\ 10^{-5}$; $a_2 = -0.04923$; $a_3 = 8.28271$;
$a_4 = 1.49300.\ 10^{-5}$; $a_5 = -0.00112$; $a_6 = 212.21416$;
$a_7 = -7.13221.\ 10^{-5}$; $a_8 = 0.047423336$; $a_9 = -8.66361$;
$a_{10} = -0.00656$; $a_{11} = 4.2685$; $a_{12} = -675.32453$;

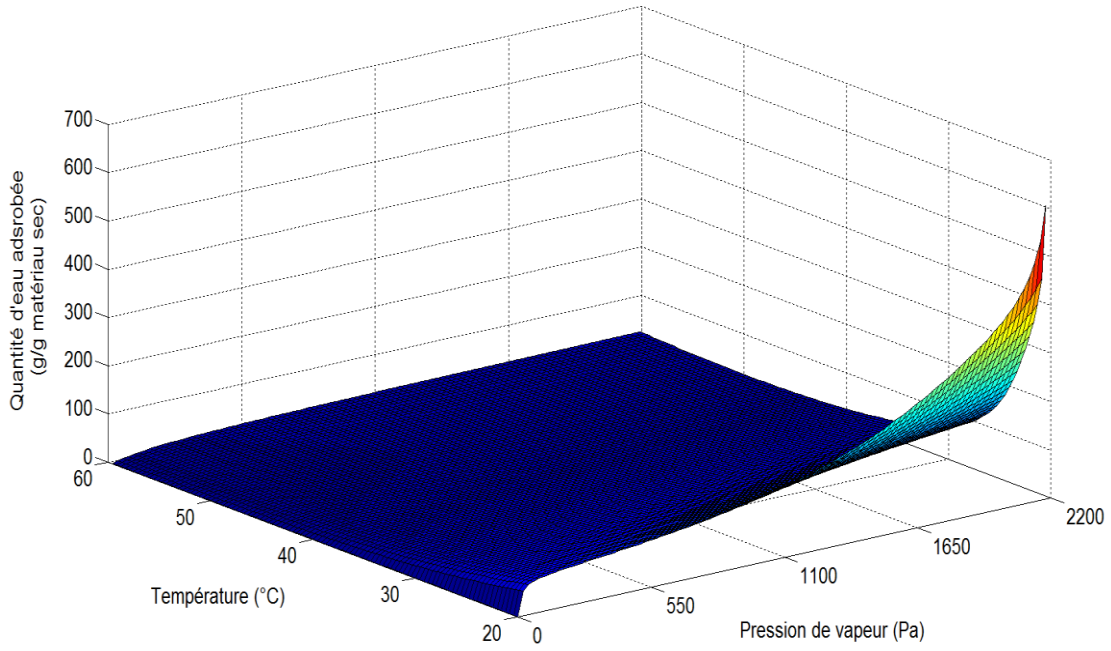


Figure 9 : Pickett isotherms of the material, based on the analysis of the experimental results

5.1.2. Complementary parameters

The ettringite-based material from the hydration of calcium sulfoaluminate cement was investigated using standard tests in the laboratory to measure physical, thermal and hygrometric properties (Table 2).

Table 2: Input parameter values

Parameter	Symbol	Value
Absorbent material: ettringite-based material		
Porosity	ε	76%
Density	ρ	420 kg/m^3
Gas permeability	K	1.44.10^{-13} m^2
Diffusion coefficient	D_v	7.14.10^{-9} m^2/s
Thermal conductivity	λ_s	0.084 W/(m.K)
Heat capacity	c_s	1260 J/(kg.K)
Sorption enthalpy	ΔH	3950 J/g_{water}
Absorbed phase: water vapour		
Dynamic viscosity	μ	10^{-5} Pa.s
Heat capacity of water vapour	c_g	2000 J/(kg.K)
Heat capacity of water liquid	c_a	4180 J/(kg.K)

Heat exchanger fluid, metal tube and absorber dimensions		
Thermal conductivity of fluid	λ_f	0.1 W/(m.K)
Thermal conductivity of metal tube	λ_m	15.6 W/(m.K)
Velocity	v	0.01 m/s
Length of the adsorbent bed	L	13 cm
Inner radius of the metal tube	R_1	1 cm
Outer radius of the metal tube	R_2	1.01cm
Outer radius of adsorbent bed	R_3	11 cm

A high thermal conductivity allows to reach a thermal equilibrium faster in storage phase and therefore to obtain a more homogeneous dehydration within the material. However, it would lead to a rapid dissipation of heat in the storage system by heat losses during the discharge phase.

More external insulation would limit heat losses in discharging phase, but will reduce the heat transfer within the material if its thermal conductivity is too low.

To sum up, a high thermal conductivity could be interesting for daily storage where short heating phase duration is required. However, a low thermal conductivity could be adapted to long-term storage where a slow and gradual regeneration phase may be sought.

5.2. Charging phase simulation

The charging phase began with the circulation of the heat transfer fluid to bring the heat into the thermochemical reactor.

5.2.1. Heat transfer fluid temperature

In order to heat the ettringite material, the heat transfer fluid (hot water) entered the metal tube at 60°C with a low velocity of 0.01 m/s, the heat spread quickly into the tube but the fluid temperature near the metal tube ($r = R_1$) had not reached uniformity even after two hours of heating (Figure 10). This is explained by the fact that the heat was transferred from the fluid to the cementitious material through the metal tube.

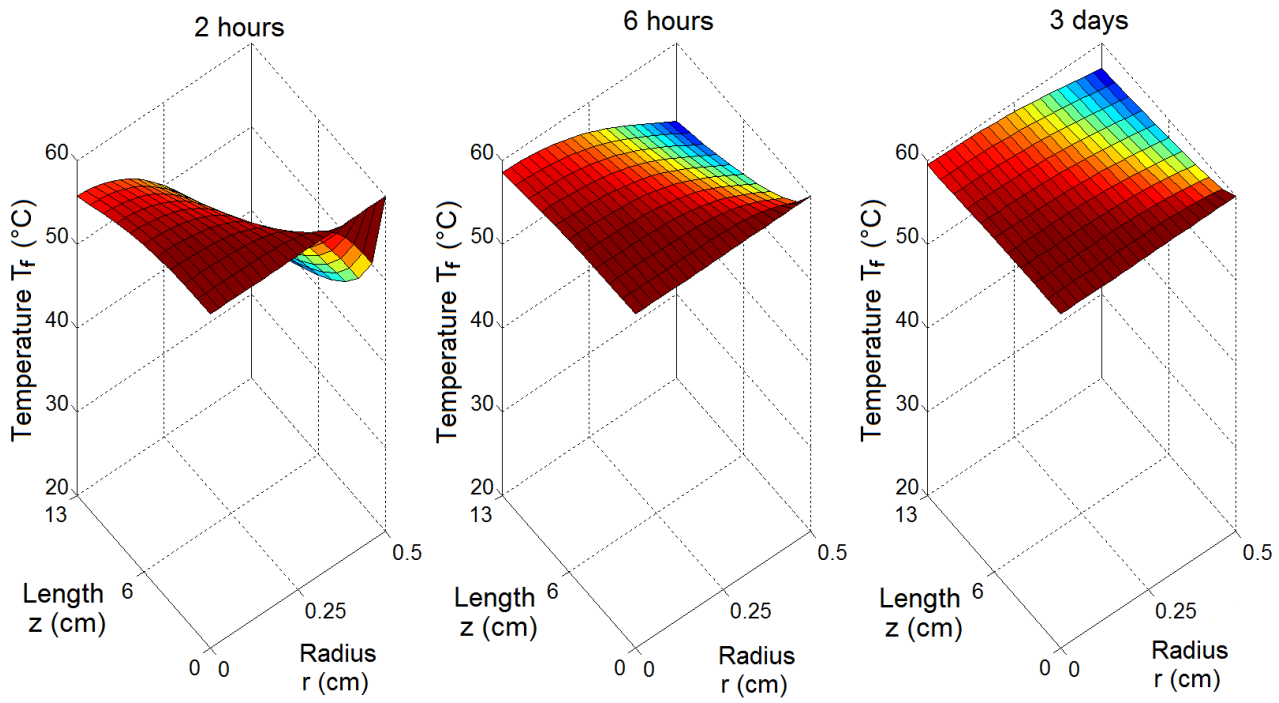


Figure 10: Heat transfer fluid temperature evolution into the metal tube during charging phase

5.2.2. Temperature in the ettringite material

The temperature increase of the material (ettringite-based material) was very slow compared to that of the heat exchanger fluid (Figure 11). The heat diffusion into the material was mainly in the radial direction from the inner cylindrical wall (metal tube, R_2) to the outer cylindrical wall (R_3). The latter was assumed adiabatic during the heating phase (Neumann boundary condition), so the low material temperature near this zone (R_3) even after two hours of heating was not related to heat loss but was due to the fact that the heat from the heat exchanger fluid (hot water) had still not reached the outer cylindrical wall. Furthermore, the slight drop in material temperature with the length of the material was due to the residence time of the heat transfer fluid in the metal tube; in fact, hot fluid moved into and out of the metal tube, at z = 0 and z = L, respectively, with a slow velocity (v =0.01 m/s) (Figure 10).

Overall temperature uniformity throughout the reactor was not reached even after three days (Figure 11). This was partially related to the low thermal conductivity of the cementitious material (λ_s = 0.084 W/(m.K)). To avoid this phenomenon, the thermal conductivity could be optimized by improving the material formulation. High thermal conductivity would be efficient for daily storage where a short duration of the heating phase is required. In contrast, low thermal conductivity would be well suited to long-term storage, where slow and gradual phases would be preferable.

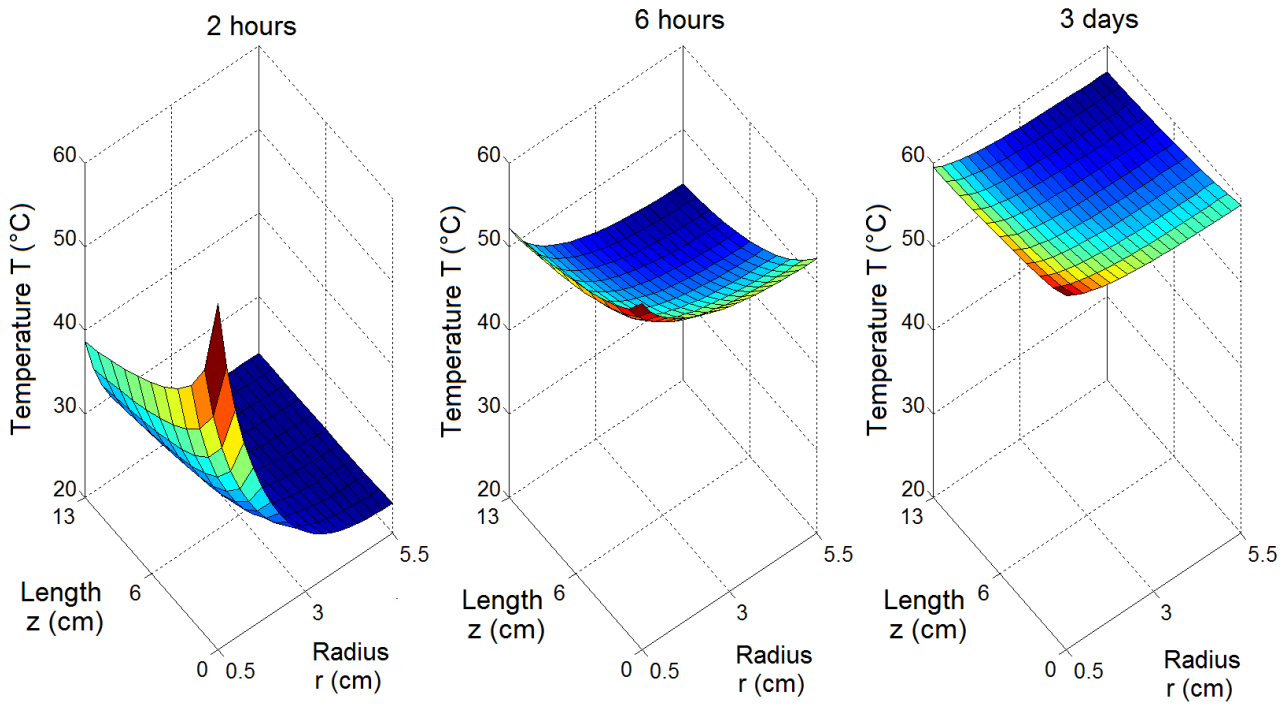


Figure 11: Temperature evolution in the material during charging phase

5.2.3. Water vapour pressure in the ettringite material

Heating the initially saturated material generated water desorption in the ettringite material. Water vapour moved outwards through the outer cylindrical face (R_3), causing the vapour pressure to decrease over time (Figure 12). Figure 12 shows a decrease of the steam pressure with the radius as the water vapour was evacuated to the outer face of the material ($p(R_3, z, t) = p_0$), while the inner surface (metal tube) remained impermeable (R_2). The heat was stored by endothermal desorption and dehydration. Thus, the heat stored in the material was composed of physical desorption heat and dehydration enthalpy when ettringite became metaettringite. This stored heat would be saved as long as the thermochemical reactor was isolated from water vapour flux, and it could be discharged either in the short term (daily, weekly storage) or long term (seasonal storage).

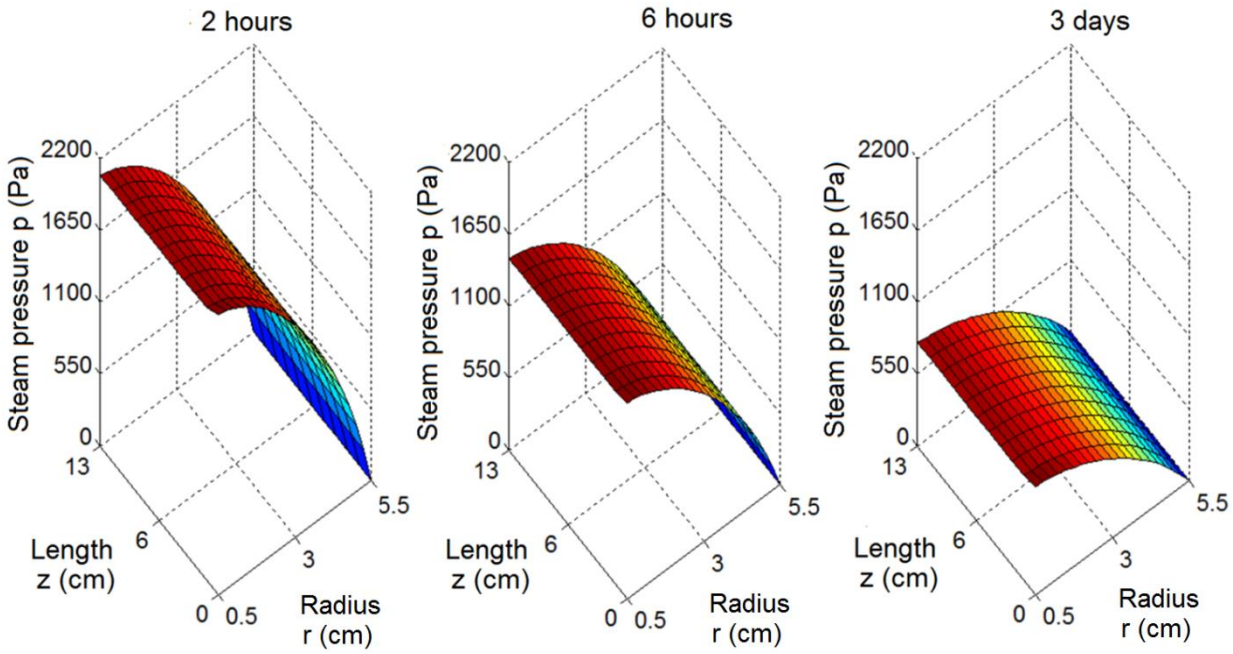


Figure 12: Water vapour pressure evolution in the material during charging phase

5.3. Discharging phase simulation

The heat discharging period began with a radial humidification of the initially dry material. This humidification stage was carried out by applying a high water vapour pressure on the outer face of the material (R_3).

5.3.1. Water vapour pressure in the ettringite material

Water vapour diffused radially into the material porosity from the outside to the inside. Figure 13 shows that the water vapour pressure in the material increased over time. The high steam pressure applied to the outer surface (R_3) tended to become uniform throughout the material over time (Figure 13).The exothermic adsorption of water vapour on the ettringite material generated gradual heat restitution. The storage generated was related to both physical and chemical processes. Humidification first caused physical adsorption of capillary water (Van der Waals bonds) and chemical rehydration of metaettringite to ettringite, by recovery of 18 water molecules per ettringite formula. The amount of heat restored was related to the amount of water adsorbed. Thus, the discharging phase can be controlled by controlling the humidification. This restitution phase could also be carried out in several steps to meet the heating demand of buildings. Exhaustion of the stored energy corresponded to the saturation of the material (maximal adsorption).

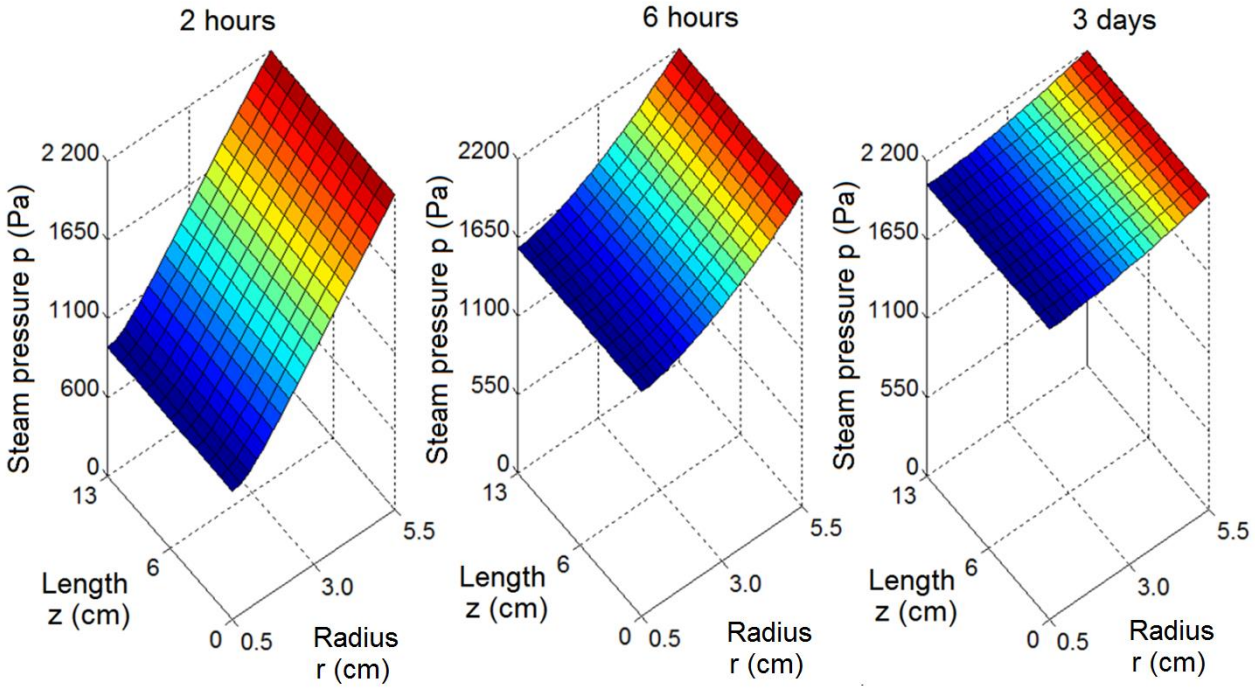


Figure 13: Water vapour pressure evolution in the material during discharging phase

5.3.2. Temperature in the ettringite material

The temperature increase at the beginning of the discharging phase was due to the exothermic adsorption of water vapour within the material (Figure 14). A temperature rise of 15K was achieved on the material outer face (R_3) after 6 hours of hydration (Figure 14). Then there was a temperature drop noted on the 3rd day because the system had evacuated the released heat via the continuous flow of cold heat transfer fluid (cold water) into the tube. This cooled the material through the metal tube and allowed the released heat to be moved out of the thermochemical reactor.

The spatial distribution of the temperature in the material was not uniform during this phase; the temperature increased with the radius and the length. The heat of the material surrounding the metal tube was transferred to the heat transfer fluid via the metal tube. During this phase, the heat transfer fluid always entered the tube at room temperature 20°C (z = 0) and its temperature increased by up to 8°C at the tube outlet.

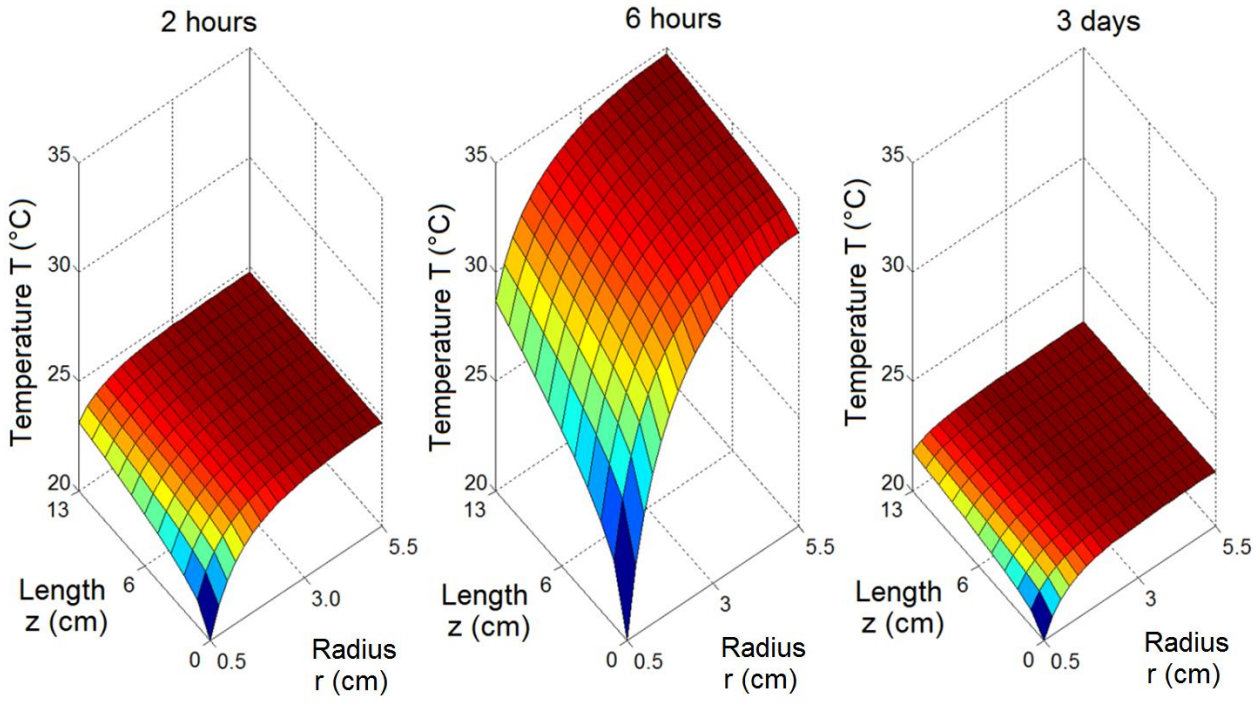


Figure 14: Temperature evolution in the material during discharging phase

5.3.3. Temperature in the metal tube

Figure 15 shows that the heat transfer fluid (cold water) used to recover the thermal energy released always entered the tube at room temperature (20°C, z = 0). Then, as the fluid moved slowly (v = 0.01 m/s) through the radial heat exchanger, its temperature increased with length to reach an increase of 8°C at the thermochemical reactor outlet. This hot fluid, recovered during the discharging phase, could be used for various applications in the building.

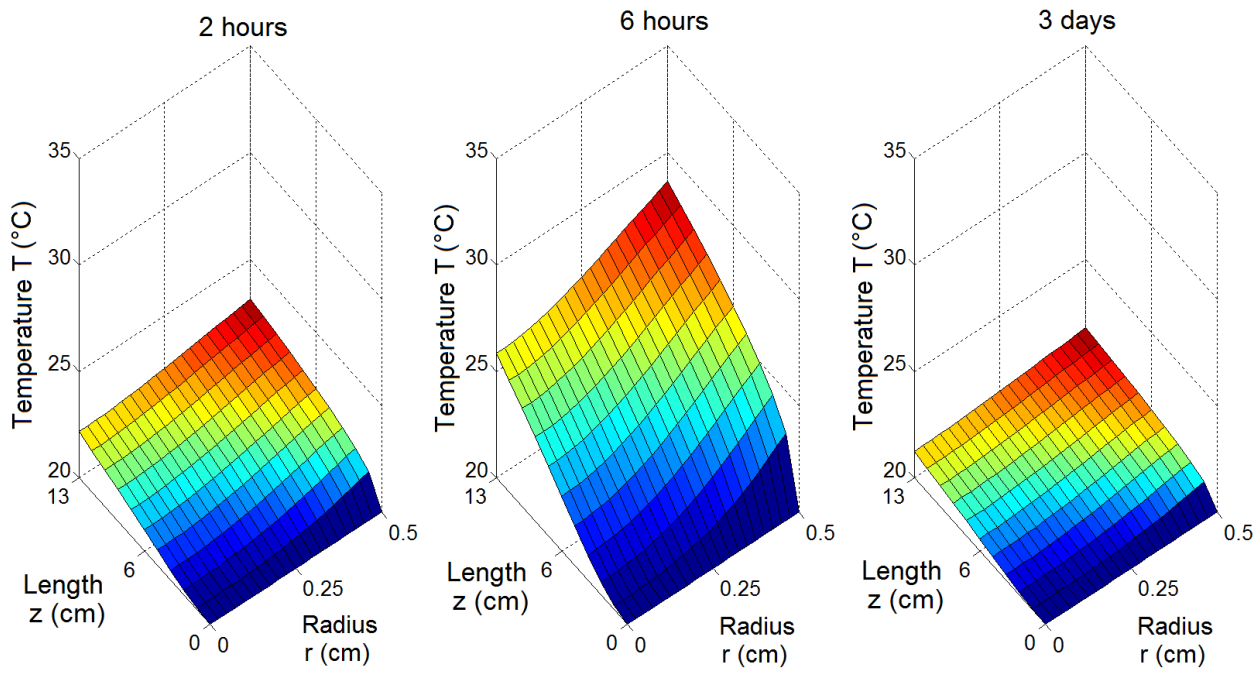


Figure 15: Evolution of heat transfer fluid temperature in the metal tube during discharging phase

The heat storage model, based on the mass and energy balance in thermochemical reactor taking the specificities of cementitious materials into account, allowed the spatiotemporal behaviour of the heat storage system to be predicted, knowing the material properties. Thus the results of this numerical study not only provided better knowledge of the material behaviour but also determined the optimal operating conditions for heat storage. This helped to build the thermochemical reaction prototype for the heat storage tests in both the charging and discharging phases. Numerical and experimental results were compared in order to validate the numerical results.

6. Prototype and experimental validation

6.1. Prototype description

The thermochemical reactor modelled and simulated was built in the laboratory. It was a cylindrical adsorber 11 cm in diameter and 13 cm long, containing ettringite material with a central metal tube 1 cm in diameter and 13 cm long (Figure 1). The cementitious material placed around the tube was protected by a water- and vapour-tight PVC cylinder. The prototype was also thermally insulated by a 10 cm thickness of glass wool and a thin layer of polystyrene at the surface. The temperature and relative humidity sensors previously inserted into the material were used to follow temperature and water vapour pressure in the reactor during the charging and discharging phases (Figure 16).

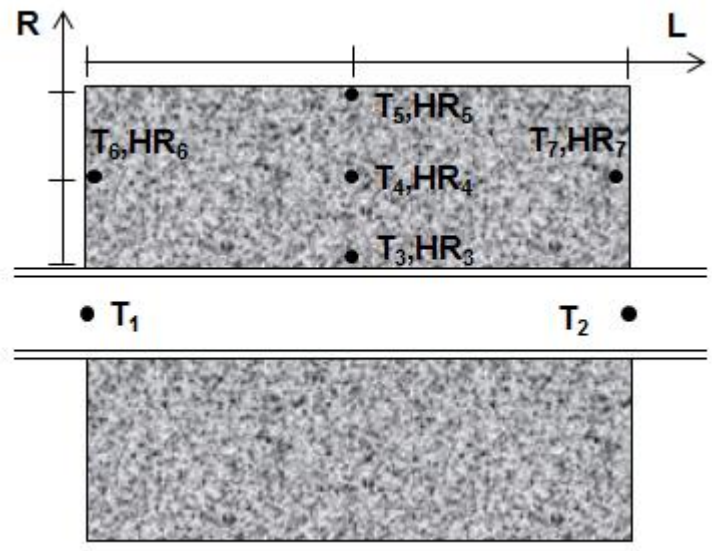


Figure 16: Position of the temperature sensors (T_1 to T_7) and relative humidity sensors (HR_3 to HR_7) in the thermochemical reactor

The positon of sensors in the thermochemical reactor and their characteristics are shown in Figure 16 and Table 3, respectively. To store the solar heat, for example, (daily or seasonal storage), it is necessary to connect the thermochemical reactor with a heat source (solar collector for example) to charge it during the storage phase. However, during the discharging phase, a humidification source was required to release heat.

Table 3: Sensor types and their uncertainty

Sensors	Temperature range	Uncertainty	Position
Type K thermocouples	0 - 100°C	± 0.5°C	1 to 7
Humidity sensors	0 - 100% RH	2 - 3 %	3 to 7

To perform the storage tests in the laboratory, the reactor was connected to a heater (electric water heater) and humidifier (bubbler) simulating heat charging and discharging, respectively (Figure 17). These two devices (heater and humidifier) did not operate simultaneously. The heater was only used during the charging phase, while the humidifier only hydrated the material during the discharging phase. The set {reactor + heat source + source of moisture} formed the heat storage system. The test bed installed in the laboratory could reproduce the storage system. It was composed of a thermochemical reactor (adsorber), an electric water heater (heater), a bubbler (humidifier), a nitrogen cylinder, and an acquisition module connected to a computer (Figure 17).

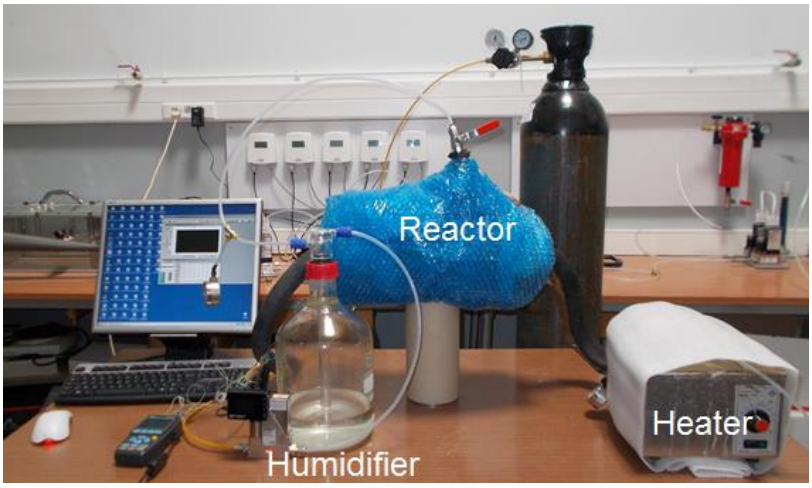


Figure 17: Test bed of heat storage

6.2. Operation of prototype during charging phase

The heater was an electric water heater in which a coiled metal tube was immersed (Figure 18). This device was connected to the heat exchanger fluid (water) circuit upstream of the reactor. The cold fluid circulated in the coiled tube to reach 60°C at the outlet of the heater, so it always went into the metal tube of the reactor at 60°C. Thus the boundary condition for fluid temperature at the metal tube inlet during the heating phase (T_f (r, 0, t) = 60°C), used in the simulation, was satisfied. The fluid (water) circulated slowly (v = 0.01 m/s) in the tube to heat the material radially through the metal tube. This heating step generated an endothermic reaction from the physical desorption and the dehydration of ettringite to metaettringite. The energy of physical desorption and that of the chemical dehydration were stored in the material.

During the charging period, the humidifier was not used. The stored heat was not recovered until ettringite material was in contact with moisture (vapour or liquid).

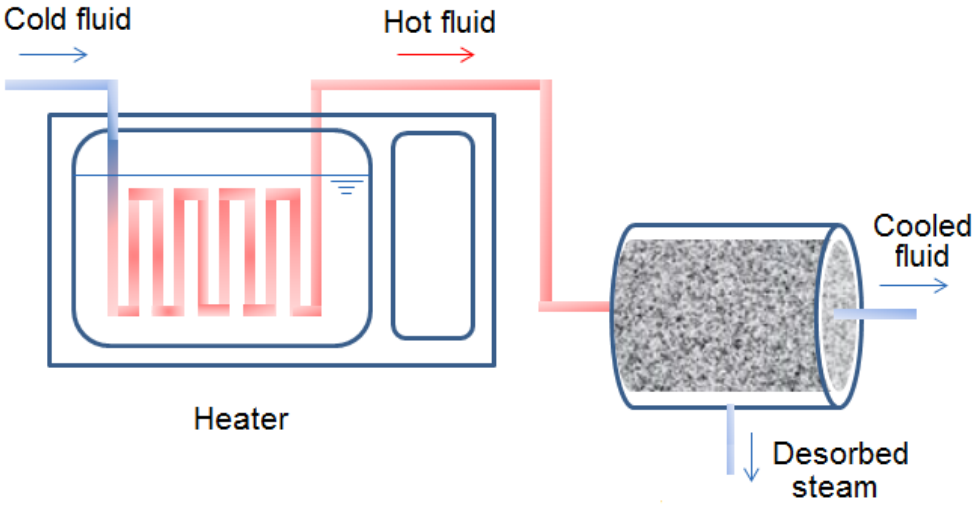


Figure 18: Operating diagram of the heater during the charging phase

The operating conditions during the charging phase are shown in Table 4.

Table 4: Operating conditions of the thermochemical reactor for the charging phase

	Charging phase	
Velocity of the fluid in the tube	0.01 m/s	
Fluid temperature at the tube inlet	60°C	*Boundary condition*
Initial temperature in the material	20°C	*Initial conditions*
Initial relative humidity in the material	100%	

To better simulate the real operating conditions of the reactor, it was necessary to cool the reactor until it reached thermal equilibrium with the atmosphere, before beginning the heat discharging phase.

6.3. Operation of prototype during discharging phase

After testing the prototype in the heating phase, its functioning in the destocking phase was studied. The latter began with the humidification of the material using a bubbler (Figure 19). To humidify the material in the discharging phase, moist nitrogen was used instead of moist air so as to avoid the presence of CO_2, because ettringite can decompose over time by carbonation [22].

The nitrogen bottle was connected to the bubbler filled with liquid water, and nitrogen gas under pressure passed through the bubbler at a rate of 2 l/min to be loaded with water vapour. It then transported the vapour into the material through the outer face of the reactor (R_3). The presence of the high relative humidity caused physical adsorption and rehydration of the material (Figure 19).

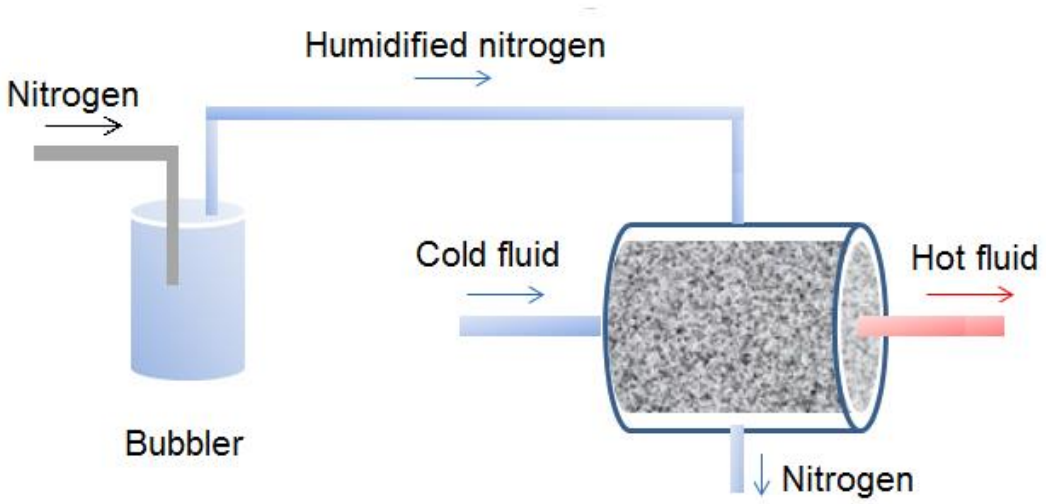


Figure 19: Operating diagram of the humidifier during discharging phase

The discharging phase test was performed using the operating conditions shown in Table 5.

Table 5: Operating conditions of the thermochemical reactor for the discharging phase

	discharging phase	
Humidified nitrogen flow	2 l/min	
Velocity of the fluid in the tube	0.01 m/s	
Fluid temperature at the tube inlet	20°C	*Boundary conditions*
Relative humidity on the material outer face	100%	
Initial temperature in the material	20°C	*Initial conditions*
Initial relative humidity in the material	0%	

6.4. Comparison of experimental and numerical results

To compare the numerical and experimental results, it was necessary to very similar hygrothermal stresses in the numerical and experimental conditions. The operating conditions used in the model were reproduced in the experiments during the storage cycle (Figure 20). The temperature and relative humidity sensors placed in the material were used to measure the evolution of state variables during charging and discharging of heat (Figure 16). These experimental results were compared with those from the numerical simulation.

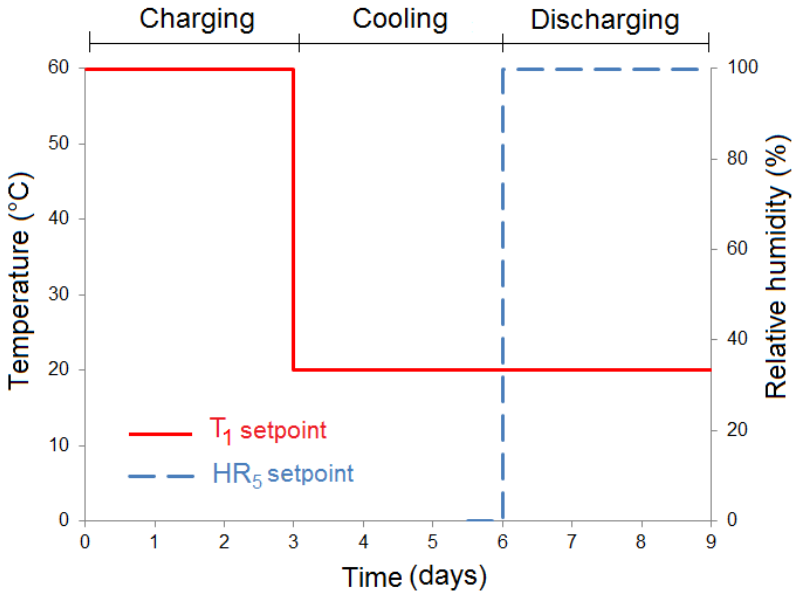


Figure 20: Setpoint of heat transfer fluid temperature at the entrance of the metal tube (T_1 setpoint) and relative humidity setpoint at the outer face of the cementitious material (HR_5 setpoint)

6.4.1. Charging phase

Type K thermocouples with an uncertainty of ± 0.5°C were placed at the tube input and output (z = 0 and z = L). The experimental evolution of the heat exchanger fluid (water) temperature in the tube was compared to that from the numerical simulation (Figure 21).

As seen previously, the heat transfer fluid (water) was heated in order to satisfy the temperature setpoint. The heater was connected to the thermochemical reactor to maintain a fluid temperature of 60°C at the metal tube input (z = 0). Figure 21 shows that the fluid temperature at the tube inlet was maintained at 60°C with a variation of ± 1.5°C.

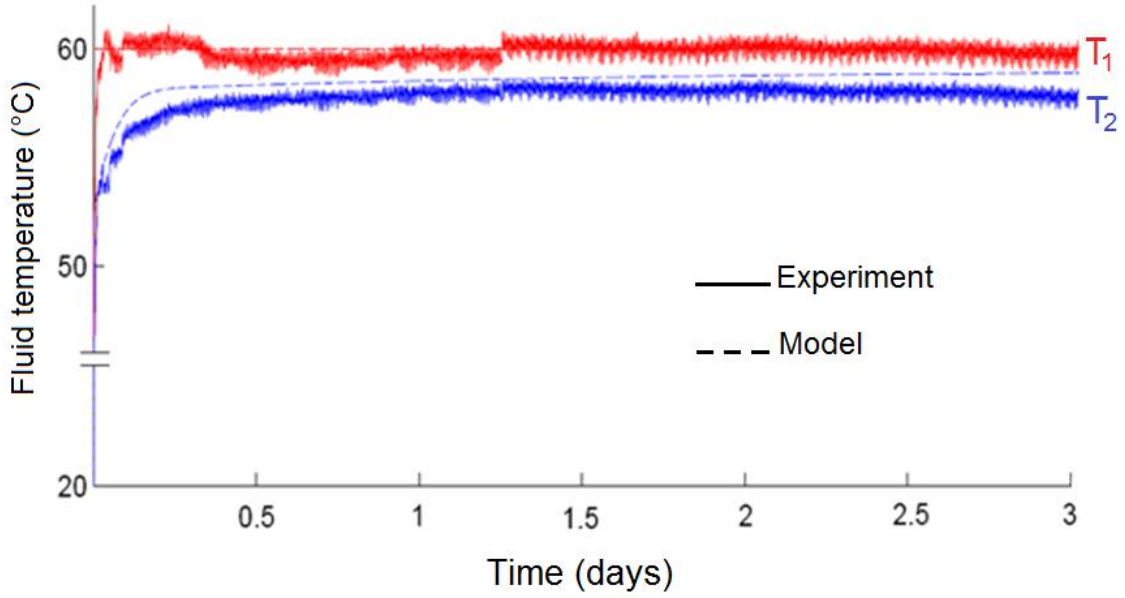


Figure 21: Experimental and numerical variation of the fluid temperature during charging phase

Figure 21 shows similar shapes between the experimental and numerical curves. These results indicate an overall agreement between experimental and numerical results, despite the noise from periodic heating cycles of the heater and uncertainties of the sensors.

As expected, the temperature of the heat exchanger fluid at the thermochemical reactor output (z = L) was less than 60°C as part of the heat was transferred to the cementitious material through the metal tube. Similarly, thermocouples placed inside the cementitious material showed a temperature rise in the material, so an increase in the amount of heat it contained heat (Figure 22).

It should be noted that it was difficult to obtain an experimental system that remained perfectly adiabatic over time. Despite the thermal insulation of the outer side of the reactor (R_3), some slight heat loss was observed. Moreover, the difference between the fluid temperature at the tube inlet and outlet (about 2°C), observed after 3 days of heating, showed that the system was not perfectly adiabatic even if heat losses were small (Figure 21).

The variation of the temperature in the material placed around the metal tube, measured by sensors 3 and 5 (Figure 16), is presented in Figure 22. Like the temperature of the fluid in the tube, that of the cementitious material increased over time but with slower kinetics. As shown in Figure 22, thermal equilibrium was reached after 24 hours of heating. This was mainly due to the low thermal conductivity (0.084 W/(m.K)) and thermal diffusivity ($1.70.10^{-7}$ m^2/s) of the cementitious material.

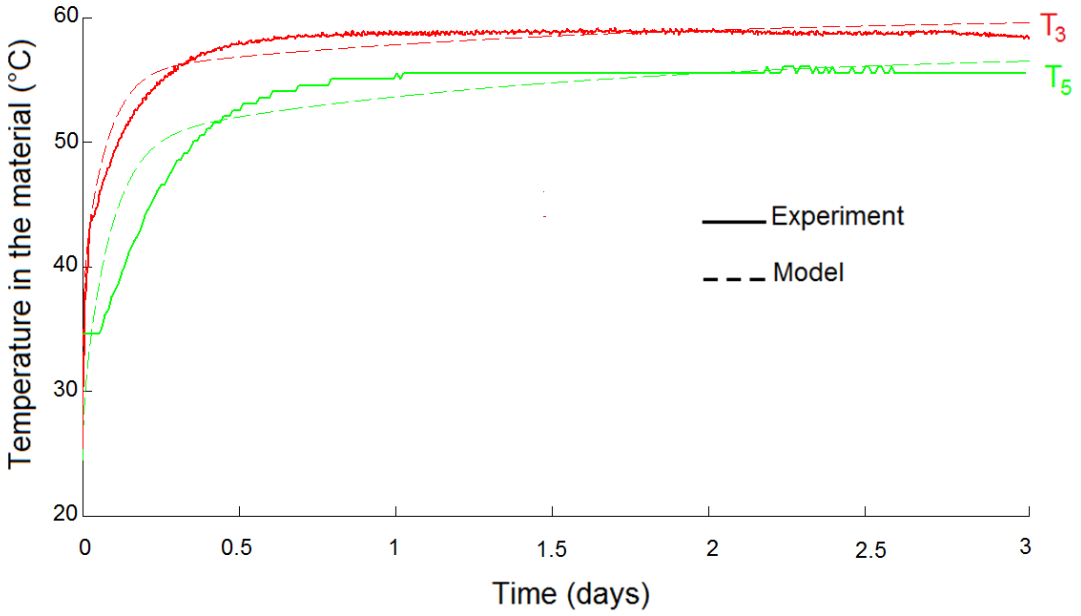


Figure 22: Experimental and numerical variation of the material temperature during charging phase

Figure 22 shows overall agreement between the model and experimental results, despite the model kinetics being slightly higher in the short-term. Several parameters can explain these differences: at the simulation level, they concern the measurement uncertainty on material properties used as model parameters, and the modelling assumptions, and, at the experiment level, they are the measurement uncertainties of sensors and devices, the homogeneity of the cementitious material, and the thermal insulation efficiency.

The heating caused desorption of the initially saturated material. The capillary water in the material porosity was desorbed first (physical bonds). Then ettringite was converted to metaettringite by loss of 18 water molecules per ettringite formula (chemical bond). The initially saturated material had become dry by the end of the heating phase. So, the stored energy was derived from a combination of physical desorption and chemical dehydration process.

The charging phase ended when the electric heater and the fluid circulation were stopped. It should be noted that the physical desorption was fast (capillary water) compared to the chemical dehydration (18 water molecules per ettringite formula) [10].The stop criterion was not based on the

relative humidity, because the chemical desorption continued gradually. The choice of storage duration (3 days of heating) was motivated by the fact that the 60°C isothermal heating for 3 days was required to completely convert ettringite to metaettringite [10].

The charging phase was followed by a cooling phase (intermediate phase) in which the sensible heat, which had raised the material temperature from room temperature (20°C) to the temperature setpoint (60°C) was lost, and the thermochemical reactor reached thermal equilibrium with its environment. To accelerate this cooling phase (intermediate phase), the fluid (cold water) flowed through the tube at 20°C to cool the material for 3 days. The material temperature returned to that of the test room (20°C). However, the heat from physical and chemical sorption remained stored in the material as long as the material was isolated from water vapour (sealing).

6.4.2. Discharging phase

The discharging phase was initiated by the material humidification; the humidification valve was connected to the bubbler, which was connected to the nitrogen cylinder. The flow of nitrogen caused water vaporization in the bubbles and then the diffusion of water vapour molecules into the material porosity. Therefore exothermic adsorption of water vapour was taking place in the material. Figure 23 shows the evolution of water vapour pressure in the material.

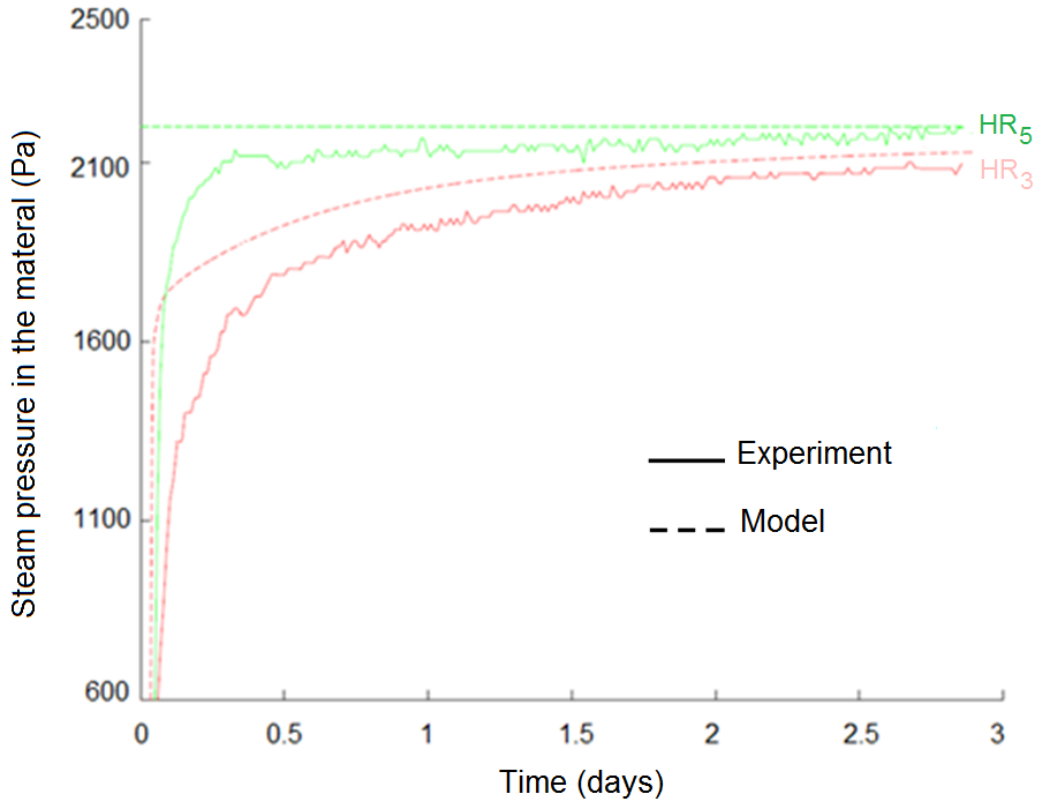


Figure 23: Experimental and numerical evolution of the vapour pressure during discharging phase

The heat from the physical adsorption and the chemical rehydration of the initially dry material was recovered by means of the slow circulation (v = 0.01 m/s) of the heat transfer fluid (cold water) in the tube. Thus, cold water always entered the metal tube at room temperature (20°C), and was then heated by the material. This was used to move the released heat outside the reactor.

Figure 24 shows an increase of the temperature of the material by as much as 12 K. The shape of the graph (heat peak) is characteristic of exothermic adsorption. The peak of sorption heat was actually a result of the synergy of physical adsorption and chemical hydration [10].

The phase shift of kinetics between the model and the experiment can be explained by the fact that the manual humidification using the bubbler was not instantaneous (Figure 23 and Figure 24). The relative humidity setpoint at the material inlet (outer surface, r = R_3) was not reached rapidly, causing a delay of the experimental exothermic adsorption compared to that of the model, where instantaneous humidification was assumed. The use of an automatic humidifier could avoid the difference in kinetics.

The maximum material temperature rise predicted by the model (13.4 K) was not achieved during the discharging phase test (12 K). This can be explained by (a) the uncertainty on the measurement of the properties, which reduced the model accuracy, and (b) the uncertainty on type K thermocouple measurements.

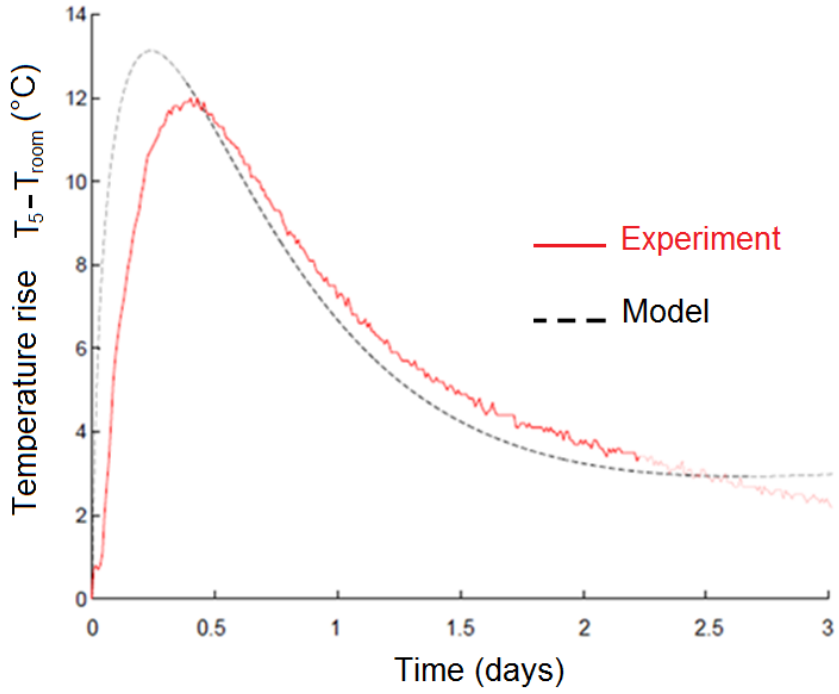


Figure 24: Experimental and numerical evolution of the material temperature during discharging phase

6.4.3. Reversibility

Many cycles were performed to study the reversibility (material heating in oven and material rehydration under water).

To assess the stability and durability of an ettringite matrix intended to be used as a storage material for heat, the reversibility during several cycles of ettringite - metaettringite conversion were investigated under the operational conditions of heat storage. The mass variation of heat-stored material over time was followed by weighing 3 specimens during a complete cycle (dehydration phase at 60°C and rehydration phase at 20°C). Isothermal conditions at 60°C and 20°C were met during the dehydration and rehydration phases, respectively. Isothermal dehydration at 60°C for 3 days led to a sudden fall in the material mass until 25% had been lost, which was an invariant level even if the heating period was extended.

The cycle of drying (heat charge for 3 days) and wetting (heat discharge during 3 days) was repeated several times in order to check the long-term reversibility of ettringite – metaettringite conversion. The results for 7 cycles of heat storage (42 days), show that 98% of the initial mass was recovered at the last cycle. The reversibility of the reaction seemed to be established. These results confirm that the topotactic conversion ettringite/metaettringite was reversible over several cycles and, consequently, the energy density of the material should not decrease over time.

6.4.4. Total energy balance of the system

The stored heat and released heat were calculated from the amount of desorbed water and adsorbed water, respectively, according to equation 18.

$$\Delta E = -(1 - \varepsilon)\Delta H(\bar{q}(t_f) - \bar{q}(t_i)) \qquad (19)$$

with $\bar{q}(t_i)$ the spatial average of the amount of water in the cementitious material at the beginning of the phase ($kg/m^3_{material}$) , $\bar{q}(t_f)$ the spatial average of the amount of water in the cementitious material at the end of the phase ($kg/m^3_{material}$), t_i the initial time of the phase, and t_f the final time of the phase.

Weighing the material before and after the charging phase allowed the amount of water desorbed or adsorbed to be deduced and the amount of stored heat to be calculated according to equation 18. Similarly, the heat released during the discharging phase was determined from the amount of water adsorbed, again according to equation 19.

Table 6: Stored heat and released heat

	Charging phase	Discharging phase
Energy stored or released ΔE (kWh/m^3)	138 kWh/m^3	61 kWh/m^3

The theoretical maximum amount of heat stored in the material corresponded to the water adsorbed at full saturation (degree of saturation S = 1). It was calculated from Equation 18 and was equal to 170 kWh/m^3, while the real amount of energy stored during the charging phase in the prototype was 138 kWh/m^3 or 81% of its optimum capacity (

Table 6). This could be due to the inhomogeneity of heating in the material, the low thermal conductivity and diffusion of the material, and probably heat loss in the reactor.

The heat released reached 61 kWh/m^3 in the discharging phase, indicating an efficiency of 44% compared to the heat stored. However with this prototype, the amount of desorbed water is higher than that of adsorbed water. If the adsorption continue until 42 days (this prototype with same size), all heat (stored) will be released, but will a very low power.

In charging phase: the heating caused desorption of the initially saturated material. The capillary water in the material porosity was desorbed first (physical bonds). Then ettringite was converted to metaettringite by loss of 18 water molecules per ettringite formula (chemical bond). The initially saturated material had become entirely dry by the end of the heating phase. So, the stored energy was derived from a combination of physical desorption and chemical dehydration process.

The discharging phase was initiated by the material humidification; the humidification valve was connected to the bubbler, which was connected to the nitrogen cylinder. The flow of nitrogen caused water vaporization in the bubbles and then the diffusion of water vapour molecules into the material porosity. Therefore exothermic adsorption of water vapour was taking place in the material. The hydration caused the conversion of metaettringite to ettringite. But the saturation was not reached in 3 days (it takes more days to reach full saturation with this prototype). In addition to this, there was some heat loss in the prototype despite the thermal insulation.

The system of heat exchange between the heat transfer fluid and the material was not optimal in this prototype. A coiled metal tube or finned tube would increase the material - fluid

exchange surface and so the energy performance. Changing from the axial tube to a coiled or finned tube in the thermochemical reactor could be a solution to increase the energy yield with a small-scale prototype (daily storage), but would lead to additional equipment costs, construction difficulties and problems of homogeneity in the material for a large-scale system (seasonal storage).

Another option may be considered: the recovery of heat directly inside the material via gas circulation, instead of the use of the axial metal tube. This option seems to be a suitable solution at both small and large scale, and could be integrated in the controlled mechanical ventilation system of buildings as a secondary heating system.

7. Conclusion

The energy and mass balance in the thermochemical reactor with ettringite material generated a system of nonlinear and coupled differential equations. This system was solved by spatial discretization using a second-order finite difference scheme then time integration using the Gear method. The simulation model using the properties of ettringite material, during the charging and discharging phases, predicted the spatial distribution of temperature and water vapour pressure in the cylindrical thermochemical reactor, and the temporal evolution of these variables, describing the reactor dynamic behaviour during a complete cycle of heat storage.

The results of this numerical study give a better understanding of the behaviour of the material in the thermochemical reactor, and also enable the operating conditions of the heat storage (range of temperature and pressure) to be predicted. These results can be considered as a design study for the construction of an experimental prototype reactor with ettringite material. The complete heat storage cycle was performed using a test bed installed in the laboratory. The release of stored heat reached 61 kWh/m^3 in the discharging phase, or a yield of 44% compared to the heat that initially entered the system.

The comparison between experimental and model results showed overall agreement, despite differences in the pressure or temperature, probably related to measurement uncertainties and experimental conditions. So the heat storage test with the thermochemical reactor prototype validated the numerical simulation and served as a proof of concept. To improve the heat performance of the reactor, a prototype without the metal tube will be studied, in which only one gas will be used as the heat transfer fluid (charge) and the humidifying fluid (discharge).

8. References

[1] B. Zalba, J.M. Marín, L.F. Cabeza, H. Mehling, Review on thermal energy storage with phase change: materials, heat transfer analysis and applications, Applied Thermal Engineering, 23 (3) (2003) 251-283.
[2] L.J. Struble, P.W. Brown, Heats of dehydration and specific heats of compounds found in concrete and their potential for thermal energy storage, Solar Energy Materials 1 (1986) 1-12.
[3] J. Van Berkel, Solar thermal storage techniques, Research commissioned by The Netherlands Agency for Energy and the Environment NOVEM, project # 143.620-935.8.
[4] I. Odler, Special Inorganic Cements, CRC Press. 416 p, ISBN 0203302117.
[5] L. Su, N. Li, X. Zhang, Y. Sun, J. Qian, Heat transfer and cooling characteristics of concrete ceiling radiant cooling panel, Applied Thermal Engineering 84 (2015) 170-179.
[6] F. Bai, C. Xu, Performance analysis of a two-stage thermal energy storage system using concrete and steam accumulator, Applied Thermal Engineering, 31 (2011) 2764-2771.
[7] A. Eddhahak-Ouni, S. Drissi, J. Colin, J. Neji, S. Care, Experimental and multi-scale analysis of the thermal properties of Portland cement concretes embedded with microencapsulated Phase Change Materials (PCMs), Applied Thermal Engineering, 64 (1–2) (2014) 32-39.
[8] J. Shi, Z. Chen, S. Shao, J. Zheng, Experimental and numerical study on effective thermal conductivity of novel form-stable basalt fiber composite concrete with PCMs for thermal storage, Applied Thermal Engineering 66 (1–2) (2014) 156-161.
[9] K. Ndiaye, S. Ginestet, M. Cyr, Development of a cementitious material for thermal energy storage at low temperature, in: Proceedings of Eurotherm Seminar Nº99: Advances in Thermal Energy Storage, May 28-30, Lleida, Spain, 2014.
[10] K. Ndiaye, Etude numérique et expérimentale du stockage d'énergie par les matériaux cimentaires, PhD Thesis, Université Paul Sabatier Toulouse, 2016.
[11] AFPC-AFREM, Méthodes recommandées pour la mesure des grandeurs associées à la durabilité, Compte rendu des journées techniques AFPC-AFREM, Toulouse, 2009.
[12] L. M. Sun, N.B. Amar, F. Meunier, Numerical study on coupled heat and mass transfers in an adsorber with external fluid heating, Heat Recovery Systems & CHP 1 (1995) 19-29.
[13] K.C. Leong, Y. Liu, Numerical modeling of combined heat and mass transfer in the adsorbent bed of a zeolite/water cooling system, Applied Thermal Engineering 16 (2004) 2359-2374.
[14] A. Mhimid, A. Jemni, S. B. Nasrallah, Étude théorique des transferts couplés de chaleur et de masse lors de la désorption du couple zéolithe 13X-eau, Revue Générale de Thermique 36 (9) (1997) 697-706.
[15] A. Mhimid, Theoretical study of heat and mass transfer in a zeolite bed during water desorption: validity of local thermal equilibrium assumption, International Journal of Heat and Mass Transfer 41 (19) (1998) 2967-2677.
[16] M. Duquesne, J. Toutain, A. Sempey, S. Ginestet, E. Palomo del Barrio, Modeling of a nonlinear thermochemical energy storage by adsorption on zeolites, Applied Thermal Engineering 1 (2014) 469-480.
[17] W. Oberkampf, C. Roy, Verification and Validation in Scientific Computing, Cambridge University Press, 2010.
[18] C.W. Gear, The automatic integration of stiff ordinary differential equations, in: A.J.H. Morrell (Ed.), In: Processing 68 North-Holland, Amsterdam, 1968, pp 187-193.
[19] C.W. Gear, The automatic integration of ordinary differential equations, Communications of the ACM 14 (3) (1971) 185-190.
[20] C.W. Gear, L.R. Petzold, ODE methods for the solution of Differential/Algebraic systems». SIAM Journal on Numerical Analysis 21 (4) (1984) 521-716.

[21] L.M. Sun, Y. Feng, M. Pons, Numerical investigation of adsorptive heat pump systems with thermal wave heat regeneration under uniform-pressure conditions, International Journal of Heat and Mass Transfer 2 (1997) 281‑293.

[22] T. Nishikawa, K. Suzuki, S. Ito, K. Sato, T. Takebe, Decomposition of synthesized etttringite by carbonation, Cement and Concrete Research 22 (1992) 6-14.

[23] D.R. Garg, D.M. Ruthven, The performance of molecular sieve adsorption columns: systems with micropore diffusion control, Chemical Engineering Science 29 (2) (1974) 571-581.

[24] H. Ahn, C-H. Lee, Effects of capillary condensation on adsorption and thermal desorption dynamics of water in zeolite 13X and layered beds, Chemical Engineering Science 59 (13) (2004) 2727-2743.

[25] I.I. El-Sharkawy, B.B. Saha, S. Koyama, K.C. Ng, A study on the kinetics of ethanol-activated carbon fiber: Theory and experiments, International Journal of Heat and Mass Transfer 49 (20) (2006) 3104-3110.

[26] I.I. El-Sharkawy, On the linear driving force approximation for adsorption cooling applications, International Journal of Refrigeration 34 (3) (2011) 667-673.

[27] L.F.Shampine, M.W. Reichelt, J.A. Kierzenka, Solving Index-1 DAEs in MATLAB and Simulink, SIAM Review 41 (1999) 538-552.

[28] G. Pickett, Modification of the Brunauer-Emmett-Teller Theory of Multimolecular Adsorption, Journal of the American Chemical Society 67 (11) (1945) 1958 – 1962.

1. Introduction 3

2. Thermochemical reactor description and principle 4

3. Mathematical model of the transfer phenomenon in the cementitious material 7

3.1. Modelling assumption 7

3.2. Energy and mass balance in the reactor 9

3.3. Boundary conditions and initial conditions 11

4. Numerical method 12

4.1. Spatial discretization and time integration 13

4.2. Numerical scheme verification 14

5. Simulation results 16

5.1. Model parameters 16

5.1.1. Sorption isotherm 16

5.1.2. Complementary parameters 18

5.2. Charging phase simulation 19

5.2.1. Heat transfer fluid temperature 19

5.2.2. Temperature in the ettringite material 20

5.2.3. Water vapour pressure in the ettringite material 21

5.3. Discharging phase simulation 22

5.3.1. Water vapour pressure in the ettringite material 22

5.3.2. Temperature in the ettringite material 23

5.3.3. Temperature in the metal tube 24

6. Prototype and experimental validation 25

6.1. Prototype description 25

6.2. Operation of prototype during charging phase 27

6.3. Operation of prototype during discharging phase 28

6.4. Comparison of experimental and numerical results 29

6.4.1. Charging phase 30

6.4.2. Discharging phase 32

6.4.3. Total energy balance of the system 34

7. Conclusion 36

8. References 36